Rigorous numerics for ODEs using Chebyshev series and domain decomposition

Jan Bouwe van den Berg, *
Ray Sheombarsing †

December 14, 2015

Abstract

In this paper we present a rigorous numerical method for validating analytic solutions of nonlinear ODEs by using Chebyshev-series and domain decomposition. The idea is to define a Newton-like operator, whose fixed points correspond to solutions of the ODE, on the space of geometrically decaying Chebyshev coefficients, and to use the so-called radii-polynomial approach to prove that the operator has an isolated fixed point in a small neighborhood of a numerical approximation. The novelty of the proposed method is the use of Chebyshev series in combination with domain decomposition. In particular, a heuristic procedure based on the theory of Chebyshev approximations for analytic functions is presented to construct efficient grids for validating solutions of boundary value problems. The effectiveness of the proposed method is demonstrated by validating long periodic and connecting orbits in the Lorenz system for which validation without domain decomposition is not feasible.

1 Introduction

In dynamical system theory one is often interested in the existence of invariant objects such as equilibria, periodic orbits, heteroclinic orbits, invariant manifolds, etc. The existence of such special orbits can reveal global information about the behavior of the dynamical system, for example through forcing theorems. The analysis of these special solutions, however, is in general difficult because of the nonlinearities in the system. Hence one usually resorts to numerical simulations. The information obtained through numerical simulation gives a lot of insight, but, unfortunately, it does not yield mathematical proofs.

The field of rigorous numerics is concerned with bridging the gap between numerical simulation and mathematically sound results. The main idea is to combine numerical simulation with analysis to establish mathematically rigorous statements. Examples of such methods can be found for instance in the CAPD software-package [1], which consists of a comprehensive C^{++}-library for validated numerical computations of a variety of dynamically interesting objects for both discrete and continuous-time dynamical systems, using interval arithmetic Lohner-type algorithms. Another well-known software package is COSY, which is capable of rigorously integrating flows of vector fields using Taylor models [2, 7].

Yet another approach is based on a parameterized Newton-Kantorovich argument, sometimes called the radii-polynomial approach. We will describe this method in full detail later in the paper. For the moment, it suffices to say that it consists of restating the problem in a fixed point formulation $T(x) = x$, and contractivity of the map T (on a ball centered at the numerical approximation of the solution) is reduced to checking a finite set of inequalities that depend on the radius of the ball (i.e. the radius is a parameter), see e.g. [14, 19, 20, 22, 23, 31].

Of particular interest for the present paper is the implementation of these ideas based on Chebyshev series introduced in [23]. Chebyshev series have, of course, long been a well-known tool

*VU University Amsterdam, Department of Mathematics, De Boelelaan 1081a, 1081 HV Amsterdam, Netherlands, email: janbouwe@few.vu.nl

†VU University Amsterdam, Department of Mathematics, De Boelelaan 1081a, 1081 HV Amsterdam, Netherlands, email: r.s.s.sheombarsing@vu.nl

in numerical analysis (see e.g. [8, 25, 29] and the references therein). Their successful applicability to *rigorous* numerics is largely due to the analogy between Chebyshev series and Fourier series, allowing for manageable analytic estimates. The idea in [23] is to expand the unknown solution u to a boundary value problem in the Chebyshev-basis on the interval $[0, L]$, and to work, for the functional analytic arguments, on the space of algebraically decaying Chebyshev-coefficients.

The fundamental restriction of the setup in [23] is that only "short" pieces of orbit may be verified this way, since for longer orbits the coefficients in the Chebyshev series decay too slowly. Hence, although the Chebyshev series, due to their similarity to Fourier series, promise to vastly improve the efficiency of rigorous numerical algorithms (compared to, for example, spline approximations) for systems of ODEs, they thus far had the major restriction of only succeeding for short time intervals. In the current paper we solve this problem by adding *domain decomposition* concepts to the picture. In particular, we describe how a combination of ideas from domain decomposition and Chebyshev expansions can be united into an integrated approach for rigorous numerical computations of solutions to boundary value problems on large intervals.

To be precise, we present a rigorous numerical procedure for solving boundary value problems (BVPs)

$$\begin{cases} \dfrac{du}{dt} = g(u, \lambda_0), & t \in [0, L], \\ \mathcal{G}\big(u(0), u(L), \lambda_1\big) = 0, \end{cases} \tag{1.1}$$

using Chebyshev series and domain decomposition. Here $g : \mathbb{R}^n \times \mathbb{R}^{n_0} \to \mathbb{R}^n$ is a polynomial vector field in an n-dimensional phase space, which may depend on a parameter $\lambda_0 \in \mathbb{R}^{n_0}$. We restrict our attention to *polynomial* vector fields for technical reasons: they allow for a relatively simple functional analytic setup, see Section 2, so that we can focus on the novel domain decomposition aspects. We note that many non-polynomial (but analytic) problems may be reformulated as a polynomial problem via change of variables and automatic differentiation techniques, see e.g. [20] and the references therein. Furthermore, for the sake of presentation, the estimates in Section 6, which are needed to validate numerical approximations of (1.1), are only developed in detail for *quadratic* polynomials. We remark that the estimates for higher-order polynomials are similar and straightforward generalizations of the quadratic bounds. The function $\mathcal{G} : \mathbb{R}^n \times \mathbb{R}^n \times \mathbb{R}^{n_1} \to \mathbb{R}^{n_b}$ represents a collection of n_b boundary conditions, which may depend on a parameter $\lambda_1 \in \mathbb{R}^{n_1}$.

In the BVP (1.1) parameters may either be fixed or determining their value may be part of the problem. This also holds for the length of the interval L, which can be predetermined or a priori unknown (as in the case of a periodic orbit). In any case, to have a locally unique solution one needs that the number n_p of *free* parameters (in λ_0, λ_1 and possibly L) is such that the number of boundary conditions balances the degrees of freedom: $n_b = n + n_p$. In the current paper we restrict our attention to such problems with locally unique solutions. We note that it is well understood how to extend the method to families of solutions via rigorous continuation techniques, see [9, 14, 18, 32].

As explained above, the first step in the strategy extends the one presented in [23]. We recast (1.1) into an equivalent zero-finding problem in terms of the Chebyshev coefficients, where we incorporate a flexible domain decomposition component in the formulation. We then compute an approximate zero by truncation, and use a Newton-like scheme to establish the existence of the orbit of interest via a contraction argument.

The proposed method differs in one additional seminal aspect from the approach presented in [23]. The approach in [23] is based on recasting (1.1) into an equivalent fixed-point problem on the space of *algebraically* decaying sequences. However, integral curves of analytic vector fields are itself analytic. Hence the associated Chebyshev coefficients decay to zero at a geometric rate rather than merely at an algebraic rate. From that perspective it is more natural to pose the equivalent fixed point problem on the space of geometrically decaying sequences, i.e., on an exponentially weighted ℓ^1-space, see Section 2. This has several advantages. The estimates for bounded linear functionals and discrete convolutions, which constitute a fundamental part of the method in this paper, are more easily derived in the geometric setting; see [19] for a detailed discussion of these issues. Hence, the more transparent expressions allow us to concentrate on the core matter of domain decomposition.

Exploiting the geometric decay of the coefficients has consequences that go beyond cosmetic aspects, since the rate of decay links directly into the way the domains in the domain decomposition

are chosen. We here give a brief overview of the ideas, while all details can be found in Section 4. We split the interval $[0, L]$ into subintervals and on each of these we write u as a Chebyshev series. The main issue is how to (optimally or naturally) choose the splitting into subintervals. The theory of Chebyshev approximations explains how the decay rate of the Chebyshev coefficients of a function is related to the location of its complex singularities in the complex plane, see e.g. [29]. Crudely stated, complex singularities which are located close to the real axis are the main cause for low decay rates. A rescaling in time, or partitioning of the domain, can be used to push the complex singularities away from the real axis thereby obtaining higher decay rates (and hence fewer Chebyshev modes are needed per domain).

The goal of domain decomposition in this context is to overcome the issue of low decay rates by partitioning the domain $[0, L]$ into a finite number m of subdomains, and to rigorously solve for the Chebyshev coefficients of $\left\{u|_{[t_{i-1},t_i]} : 1 \leq i \leq m\right\}$ simultaneously. The idea is to determine a grid $\{0 = t_0 < t_1 \ldots < t_m = L\}$ such that each piece $u|_{[t_{i-1},t_i]}$ of the orbit can be accurately approximated with a relatively small number of modes. In Section 4 we present a heuristic procedure for determining a grid for which the decay rates of the Chebyshev coefficients on each subdomain are (approximately) uniform over the subdomains. By choosing m appropriately, this (uniform) decay is sufficiently rapid to obtain accurate approximations with a relatively small number of Chebyshev modes on each subinterval, so that a succesfull rigorously verified computation may ensue. The procedure is based on examining the complex singularities of the orbit to be validated by using a robust rational interpolation scheme developed in [26, 27]. In Section 5.2 we illustrate that domain decomposition based on the location of the complex singularities significantly enhances the global improvement of the decay rates in a way that cannot be achieved by merely using uniform grids.

Before proceeding with a short description of some concrete results that illustrate how domain decomposition significantly enhances the applicability of Chebyshev series in computer-assisted proofs, a few remarks concerning the literature are in order. The literature on solving boundary value problems is vast, and an overview, even when restricting to rigorous computer-assisted approaches, is far beyond the scope of this paper. Let us, however, mention a few key papers to briefly sketch what kind of methods have been developed by the rigorous numerics community.

In [3, 4, 10, 16, 37] functional analytic methods, similar in spirit to ours, are used to solve BVPs: the differential equation is reformulated into an equivalent fixed-point problem and is solved by verifying the conditions of the Contraction Mapping Principle with the aid of a computer. Fundamentally different approaches based on topological rather than functional analytic methods, such as the Conley-index and covering relations, have been proven to be very effective as well (see e.g. [5, 13, 17, 36]), especially when combined with high-accuracy interval-arithmetic integration techniques (see e.g. [6, 24]). Finally, let us also mention the method in [12] based on shadowing and fixed point arguments.

To demonstrate the effectiveness of our method we have validated "long" connecting and periodic orbits in the Lorenz system

$$\frac{du}{dt} = \begin{pmatrix} \sigma(u_2 - u_1) \\ u_1(\rho - u_3) - u_2 \\ u_1 u_2 - \beta u_3 \end{pmatrix},$$

where $\sigma, \beta, \rho \in \mathbb{R}$ are parameters. We set $\beta = \frac{8}{3}$, $\sigma = 10$, and let $\rho > 1$. The parameter values are referred to as classical if $\rho = 28$. All the computations presented below have been implemented in MATLAB, using the INTLAB package [28] for the necessary interval arithmetic, and the CHEBFUN package [15] to construct the required Chebyshev approximations. The code is available at [34].

Application 1. We have proven the existence of a transverse heteroclinic orbit between hyperbolic equilibria in the classical Lorenz system. The implementation in [22], which in spirit is very similar to the one discussed in the present paper, except that splines are used instead of Chebyshev polynomials, was not powerful enough to verify the heteroclinic orbit for the classical parameter values. For these parameter values it turns out that the connecting orbit cannot be verified by using a Chebyshev series on a single domain, hence domain decomposition is essential. The Lorenz system has three hyperbolic equilibria, namely the origin and $q^{\pm} := (\pm\sqrt{\beta(\rho-1)}, \pm\sqrt{\beta(\rho-1)}, \rho - 1)$, which are commonly referred to as the positive and negative eye. A connecting orbit from q^+ to

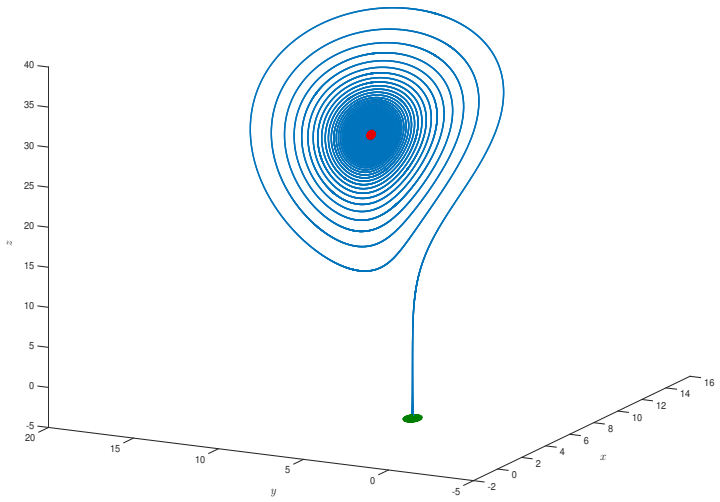

Figure 1.1: The connecting orbit from the positive eye to the origin in the Lorenz equation with classical parameters. The time of flight between the local (un)stable manifolds is $L = 30$. The geometric objects colored in red and green are representations of $W^s_{\text{loc}}(q^+)$ and $W^u_{\text{loc}}(\mathbf{0})$, respectively.

the origin is characterized by

$$\begin{cases} \dfrac{du}{dt} = g(u), & t \in [0, L], \\ u(0) \in W^u_{\text{loc}}(q^+), \\ u(L) \in W^s_{\text{loc}}(\mathbf{0}), \end{cases} \tag{1.2}$$

where $L > 0$ is the integration time required to travel from the local unstable manifold $W^u_{\text{loc}}(q^+)$ of q^+ to the local stable manifold $W^s_{\text{loc}}(\mathbf{0})$ of the origin. The local invariant manifolds can be parameterized using the method in [22, 33] to obtain rigorously validated descriptions of explicit boundary conditions that supplant the statements $u(0) \in W^u_{loc}(q^+)$ and $u(L) \in W^s_{loc}(\mathbf{0})$, see Section 5.4. The system (1.2) is thus reduced to a BVP of the type (1.1).

We established the existence of an isolated solution of (1.2) for $L = 30$ time units by using a grid consisting of $m = 55$ subdomains. The orbit is shown in Figure 1.1. The C^0-bound for the error between the exact and numerical approximation was of order 10^{-9}. The reader is referred to Section 5.4 for the details.

Application 2. We have validated a periodic orbit of period $L \approx 25.03$ on the Lorenz attractor for the classical parameter values. We note that L is a parameter and $\mathcal{G}$ consists of $u(0) - u(L) = 0 \in \mathbb{R}^3$ plus a phase condition ($u(0)$ lies in a certain Poincaré section, see Section 5.2). The orbit is shown in Figure 1.2(a). The C^0-bound for the error between the numerical approximation and the exact solution was of order 10^{-10}. Rather than pushing for extremely long orbits (which have already successfully been obtained via high-precision arithmetic [6]), this periodic orbit is primarily meant as an illustration of the typical behavior of the domain decomposition algorithm. In Figure 1.2(b) the size of the Chebyshev coefficients on all domains (as determined by the algorithm described in Section 4) is shown simultaneously. This showcases the fact that the algorithm determines a grid such that the decay rate is uniform.

Application 3. As a third application we considered a family of periodic orbits parameterized by ρ, accumulating to a homoclinic orbit to the origin at $\rho_{\text{hom}} \approx 13.93$. In particular, the periods of the periodic orbits tend to infinity as $\rho \downarrow \rho_{\text{hom}}$, and it becomes increasingly hard to validate the solution. Indeed, the goal of this example is to push our method to the edge of its current applicability. With the orbits spending a lot of time near the equilibrium, the algorithm for

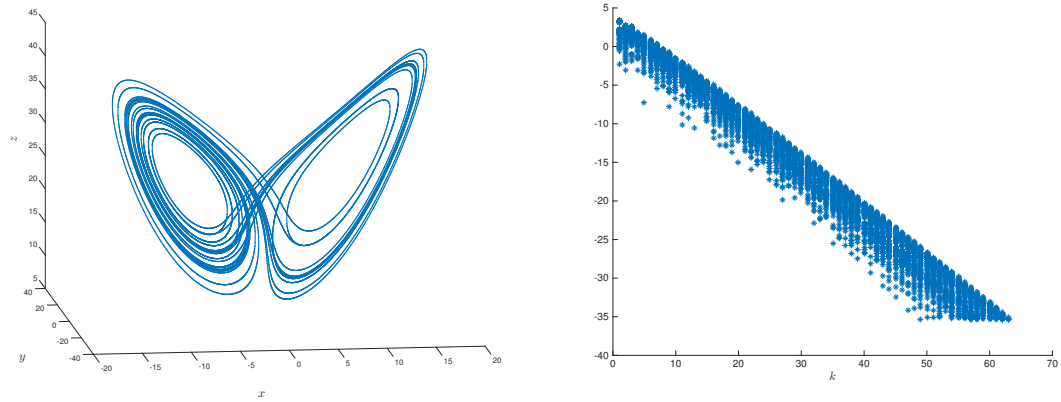

(a) (b)

Figure 1.2: (a) A periodic orbit on the Lorenz attractor of period $L \approx 25.03$ validated with $m = 35$ subdomains. (b) A semi-logarithmic plot of the coefficients in the Chebyshev series on all subdomains for the three components of the solution.

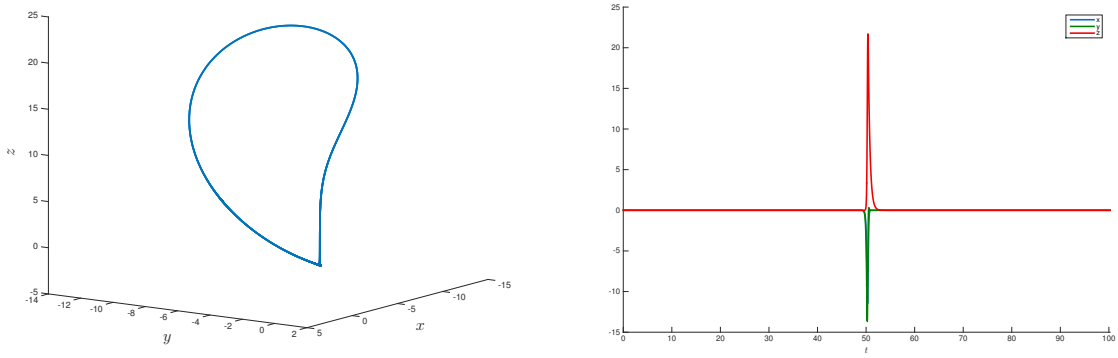

(a) (b)

Figure 1.3: (a) A typical periodic orbit near the homoclinic connection. The period of the orbit is $L \approx 100.25$. Notice the sharp turn of the orbit near the origin. (b) The x, y and z components of the orbit. The three components are fairly flat for a relatively long time. These flat parts correspond to the part of the orbit near the equilibrium where the dynamics are slow.

determining the domain decomposition based on the estimated location of the poles turns out to still work well for the part of the orbit that describes the near-homoclinic excursion, but not so well in the neighborhood of the equilibrium, see Section 5.3.1 for a more detailed discussion. Furthermore, the problem becomes increasingly ill-conditioned as ρ approaches ρ_{hom}. This is remedied by considering ρ as a free parameter rather than a fixed one, and adding a pseudo-arclength continuation type equation, see Section 5.3.1.

A typical validated periodic orbit near the homoclinic orbit for ρ close to ρ_{hom} is shown in Figure 1.3(a). It has two geometrically distinct parts: it spends a long time close to the equilibrium where the components are near-constant, see Figure 1.3(b), while the peak corresponds to the relatively short excursion into phase space. The grid is uniform on the flat part of the solution (where very few modes are used per domain), and the grid is non-uniform in the peak (where many modes are used per domain), see Section 5.3.1 for details.

This paper is organized as follows. We begin by briefly introducing the necessary background on Chebyshev series in Section 2. The setup for the rigorous verification of the numerical computations in the domain decomposition context is described in Section 3. The accompanying estimates

are postponed to Section 6 as not to break the flow of the arguments. In Section 4 we discuss the algorithm for finding a domain decomposition that leads to uniform decay of the Chebyshev coefficients. Section 5 deals with the three applications summarized above. Finally, in Section 6 we first develop the full details of the estimates for the case of periodic boundary conditions, and then give the modifications required for the non-periodic boundary conditions that are used in some of the presented applications.

2 Preliminaries

2.1 Chebyshev series

The reader is referred to [29] for all proofs and a more comprehensive introduction into the theory of Chebyshev approximations. Here we summarize the properties needed for our method.

The Chebyshev-polynomials $T_k : [-1,1] \to \mathbb{R}$ of the first kind can be defined by the relation $T_k(\cos\theta) = \cos(k\theta)$, where $k \in \mathbb{N}_0$ and $\theta \in [0,\pi]$. As suggested by this definition, the Chebyshev series associated to the Chebyshev polynomials $(T_k)_{k=0}^{\infty}$ constitute a non-periodic analog of Fourier-cosine series. In particular, Chebyshev and Fourier-cosine series have similar convergence properties. For instance, any Lipschitz continuous function admits a unique Chebyshev expansion. The following proposition describes the decay of the Chebyshev coefficients of an analytic function.

Proposition 1. *Suppose $u : [-1,1] \to \mathbb{R}$ is analytic and let*

$$u = a_0 + 2\sum_{k=1}^{\infty} a_k T_k$$

be its Chebyshev expansion. Let $E_\nu \subset \mathbb{C}$ denote an open ellipse with foci ± 1 to which u can be analytically extended, where $\nu > 1$ is the sum of the semi-major and semi-minor axis. If u is bounded on E_ν, then $|a_k| \leq M\nu^{-k}$ for all $k \in \mathbb{N}_0$, where $M = \sup_{z\in E_\nu} |u(z)|$.

Remark 1. The largest such ellipse E_ν is referred to as the Bernstein ellipse associated to u.

The product of two Chebyshev series is (in direct analogy with Fourier series) described by a discrete convolution, as expressed by the next proposition.

Proposition 2. *Suppose $u, v : [-1,1] \to \mathbb{R}$ are Lipschitz continuous and let*

$$u = a_0 + 2\sum_{k=1}^{\infty} a_k T_k, \quad v = b_0 + 2\sum_{k=1}^{\infty} b_k T_k,$$

be the associated Chebyshev expansions. Then

$$u \cdot v = c_0 + 2\sum_{k=1}^{\infty} c_k T_k, \qquad \text{where} \qquad c = a * b := \sum_{\substack{k_1+k_2=k \\ k_1,k_2\in\mathbb{Z}}} a_{|k_1|} b_{|k_2|}.$$

Furthermore, we state an identity which will be useful for computing the derivative of a Chebyshev-series:

$$\frac{dT_k}{dx}(x) = \frac{k}{1 - T_2(x)}\left(T_{k-1}(x) - T_{k+1}(x)\right), \quad k \in \mathbb{N}. \tag{2.1}$$

Finally, we have the product formula

$$T_{k_1} T_{k_2} = \frac{1}{2}(T_{k_1+k_2} + T_{|k_1-k_2|}). \tag{2.2}$$

As we will be solving boundary value problems, we observe that $T_k(1) = 1$ and $T_k(-1) = (-1)^k$.

2.2 Sequence spaces

The functional analytic reformulation of (1.1) in terms of the Chebyshev coefficients is posed on a weighted ℓ^1 space. More precisely, in light of Proposition 1, we define the space

$$\ell^1_{(\nu,n)} := \left\{ (a_k)_{k\in\mathbb{N}_0} : a_k \in \mathbb{R}^n,\ \left|[a_0]_j\right| + 2\sum_{k=1}^{\infty} \left|[a_k]_j\right| \nu^k < \infty,\ 1 \le j \le n \right\},$$

where $[a_k]_j$ denotes the j-th component of $a_k \in \mathbb{R}^n$ and $\nu > 1$ is a given weight, endowed with the norm

$$\|a\|_{(\nu,n)} := \max_{1\le j\le n} \left\{ \left|[a_0]_j\right| + 2\sum_{k=1}^{\infty} \left|[a_k]_j\right| \nu^k \right\}.$$

We shall write $\ell^1_\nu := \ell^1_{(\nu,1)}$ and $\|\cdot\|_\nu = \|\cdot\|_{(\nu,1)}$. The convolution $a*b$ of two vector-valued sequences $a, b \in \ell^1_{(\nu,n)}$ is defined component-wise.

A particularly important reason for choosing the above norm is that it induces a natural Banach algebra structure on $\ell^1_{(\nu,n)}$ with respect to the discrete convolution:

Proposition 3. *The space* $\left(\ell^1_{(\nu,n)},\ *\right)$ *is a Banach algebra. In particular*

$$\|a * b\|_{(\nu,n)} \le \|a\|_{(\nu,n)} \|b\|_{(\nu,n)}$$

for any $a, b \in \ell^1_{(\nu,n)}$.

Finally, we state an elementary result about the dual of ℓ^1_ν which will be used extensively throughout this paper. Let $\{\varepsilon_l\}_{l=0}^\infty$ be the set of "corner points" of the unit one ball in ℓ^1_ν:

$$(\varepsilon_0)_k := \begin{cases} 1 & k = 0 \\ 0 & k > 0, \end{cases} \qquad \text{and} \qquad (\varepsilon_l)_k := \begin{cases} \frac{1}{2\nu^l} & k = l \\ 0 & k \ne l, \end{cases} \quad \text{for } l \in \mathbb{N}. \tag{2.3}$$

Then we have the following characterization of the dual of ℓ^1_ν.

Lemma 1. *Let* $\psi \in \left(\ell^1_\nu\right)^*$, *then*

$$\|\psi\|^*_\nu = \sup_{l\in\mathbb{N}_0} |\psi(\varepsilon_l)|.$$

3 Rigorous numerics for periodic orbits

In this section we introduce a rigorous numerical method for solving a special case of (1.1), namely we consider the problem of validating a periodic orbit. The reason why we have chosen to present the details of the method for periodic orbits is only for the sake of clarity, and it will be shown in Section 5 how one can adapt the procedure to deal with other types of BVPs.

Since periodic orbits are invariant under translations in time, we need to introduce an additional *phase condition* in order to isolate the periodic orbit of interest. Note that a periodic orbit can be characterized by the following BVP:

$$\begin{cases} \dfrac{du}{dt} = \dfrac{1}{\omega} g\left(u\right), & t \in [0,1], \\ u\left(0\right) = u\left(1\right), \\ \langle v_0, u_0 - u\left(0\right)\rangle = 0, \end{cases} \tag{3.1}$$

where $\omega > 0$ is the frequency of u, and $u_0, v_0 \in \mathbb{R}^n$ are fixed. The vectors u_0 and v_0 define a Poincaré section through which the periodic orbit u is required to pass at time $t = 0$ (i.e. the phase condition). Note that the frequency ω is a-priori unknown and must be included as an additional variable to solve for.

We start by recasting the problem into an equivalent zero finding problem of the form $F(x) = 0$ in terms of the Chebyshev coefficients. Next, we construct a Newton-like operator T for F based at an approximate zero $\hat{x}$ obtained via numerical simulation. Finally, we use a parameterized Newton-Kantorovich method to determine a finite number of explicit inequalities, which can be rigorously verified with the aid of a computer, in order to establish that T is a contraction on a neighborhood of the approximate solution $\hat{x}$.

3.1 Chebyshev operator for periodic orbits

In this section we reformulate (3.1) as an equivalent equation of the form $F(x) = 0$ by performing domain decomposition and using a Chebyshev expansion on each subdomain. Let

$$\mathscr{P}_m := \{t_0 = 0 < t_1 < \ldots < t_m = 1\}$$

be any partition of $[0, 1]$, where $m \in \mathbb{N}$ is the mesh size. Then (3.1) is equivalent to

$$(\mathbf{P}_1) \begin{cases} \dfrac{du_1}{dt} = \dfrac{1}{\omega} g\left(u_1\right), & t \in [0, t_1], \\ u_1(0) - u_m(1) = 0, \\ \langle v_0, u_0 - u_1(0) \rangle = 0, \end{cases}$$

$$(\mathbf{P}_i) \begin{cases} \dfrac{du_i}{dt} = \dfrac{1}{\omega} g\left(u_i\right), & t \in [t_{i-1}, t_i], \\ u_i\left(t_{i-1}\right) = u_{i-1}\left(t_{i-1}\right), \end{cases} \quad \text{for } 2 \le i \le m.$$

Note that each u_i (if it exists) is analytic, since g is assumed to be polynomial (say of degree N_g):

$$g(u) = \sum_{|\alpha|=0}^{N_g} g_\alpha u^\alpha,$$

where $g_\alpha \in \mathbb{R}^n$. Here $\alpha = (\alpha_1, \ldots, \alpha_n)$ is the usual multi-index, with $|\alpha| = \alpha_1 + \cdots + \alpha_n$. Therefore, the Chebyshev expansion

$$u_i = a_0^i + 2\sum_{k=1}^{\infty} a_k^i T_k^i, \quad a_k^i \in \mathbb{R}^n, \tag{3.2}$$

is unique and converges uniformly to u_i on $[t_{i-1}, t_i]$. Furthermore, the coefficients $\left(\left[a_k^i\right]_j\right)_{k\in\mathbb{N}_0}$, where $1 \le j \le n$, decay geometrically to 0 as $k \to \infty$ by Proposition 1. In particular, there exist numbers $(\nu_i)_{i=1}^m$, where each $\nu_i > 1$, such that $\left[a^i\right]_j \in \ell^1_{\nu_i}$ for all $1 \le i \le m$, $1 \le j \le n$. In the remainder of this section the weights $\nu = (\nu_i)_{i=1}^m$ are assumed to be fixed.

To obtain a reformulation of $(\mathbf{P}_i)_{i=1}^m$ in terms of the coefficients a^i, first observe that

$$g \circ u_i = c_0^i + 2\sum_{k=1}^{\infty} c_k^i T_k^i,$$

where

$$c^i = \sum_{|\alpha|=0}^{N_g} g_\alpha \left[a^i\right]_1^{\alpha_1} * \ldots * \left[a^i\right]_n^{\alpha_n}, \tag{3.3}$$

$1 \le i \le m$, $1 \le j \le n$, by Proposition 2. Note that c^i is a function of a^i. In particular, $c^i : \ell^1_{(\nu_i,n)} \to \ell^1_{(\nu_i,n)}$, since

$$\left\| \left[c^i\right]_j \right\|_{\nu_i} \le \sum_{|\alpha|=0}^{N_g} \left| \left[g_\alpha\right]_j \right| \prod_{l=1}^{n} \left\| \left[a^i\right]_l \right\|_{\nu_i}^{\alpha_l} < \infty, \tag{3.4}$$

for all $1 \leq j \leq n$, by Proposition 3. We shall write $c^i = c^i(a^i)$ whenever we need to emphasize this dependency in a more explicit way.

Substitution of the Chebyshev expansion of u_i into the differential equation in $\mathbf{P}_i$ yields

$$\frac{du_i}{dt} = 2\sum_{k=1}^{\infty} a_k^i \frac{dT_k^i}{dt} = g \circ u_i = c_0^i + 2\sum_{k=1}^{\infty} c_k^i T_k^i. \tag{3.5}$$

By differentiating the Chebyshev polynomials, equating coefficients of the same order on the left- and right-hand side of (3.5), and using (2.1) and (2.2), or more directly using $T_k(\cos\theta) = \cos(k\theta)$, one obtains an equivalent formulation of the differential equation in terms of the coefficients $\left(a_k^i\right)_{k\in\mathbb{N}_0}$:

$$\omega k a_k^i = \frac{t_{i+1} - t_i}{4}(c_{k-1}^i - c_{k+1}^i).$$

The equivalent equations for the boundary conditions are obtained in a similar fashion. In particular, substitution of the Chebyshev expansion of u_i into the phase condition yields

$$\langle v_0, u_0\rangle - \left\langle v_0, a_0^1\right\rangle - 2\sum_{k=1}^{N_1} (-1)^k \left\langle v_0, a_k^1\right\rangle = 0,$$

where we have, without loss of generality, adapted it to depend only on finitely many coefficients (this simplifies the estimates). In practice, N_1 will be the number of modes up to which a^1 is computed numerically.

We are now ready to define the desired map F:

Definition 1 (Chebyshev operator for periodic orbits)**.** Let $\nu = (\nu_i)_{i=1}^m$ and $\tilde{\nu} = (\tilde{\nu}_i)_{i=1}^m$ be collections of weights such that $1 < \tilde{\nu}_i < \nu_i$ for all $1 \leq i \leq m$. The Chebyshev operator for periodic orbits is the map $F : \mathbb{R} \times \prod_{i=1}^m \ell^1_{(\nu_i,n)} \to \mathbb{R} \times \prod_{i=1}^m \ell^1_{(\tilde{\nu}_i,n)}$ defined by

$$F(x) := \left(f_0\left(a^1\right), f_1\left(\omega, a^1, a^m\right), f_2\left(\omega, a^1, a^2\right), \ldots, f_m\left(\omega, a^{m-1}, a^m\right)\right),$$

where $x = \left(\omega, a^1, \ldots, a^m\right)$, $f_0 : \ell^1_{(\nu_1,n)} \to \mathbb{R}$, and $f_i : \mathbb{R} \times \ell^1_{(\nu_{i-1},n)} \times \ell^1_{(\nu_i,n)} \to \ell^1_{(\tilde{\nu}_i,n)}$, are given by

$$f_0\left(a^1\right) := \langle v_0, u_0\rangle - \left\langle v_0, a_0^1\right\rangle - 2\sum_{k=1}^{N_1} (-1)^k \left\langle v_0, a_k^1\right\rangle,$$

$$f_i\left(\omega, a^{i-1}, a^i\right) := \begin{cases} a_0^i - a_0^{i-1} + 2\sum_{k=1}^{\infty}\left((-1)^k a_k^i - a_k^{i-1}\right), & k = 0, \\ \omega k a_k^i - \dfrac{t_i - t_{i-1}}{4}\left(c_{k-1}^i - c_{k+1}^i\right), & k \in \mathbb{N}, \end{cases}$$

for $i = 1, \ldots, m$, where we set $a^0 = a^m$.

Remark 2. If $a^i \in \ell^1_{(\nu_i,n)}$, then $\left(k a_k^i\right)_{k\in\mathbb{N}_0} \in \ell^1_{(\tilde{\nu}_i,n)}$ for any $1 < \tilde{\nu}_i < \nu_i$.

By construction, we now have the following:

Proposition 4. *$F(x) = 0$ if and only if the functions $\left\{u_i = a_0^i + 2\sum_{k=1}^{\infty} a_k^i T_k^i : 1 \leq i \leq m\right\}$ constitute a periodic orbit of g.*

3.2 Finite Dimensional Reduction

In this section we explain how to discretize the equation $F(x) = 0$ in order to compute a finite-dimensional approximate solution of (3.1). We start by introducing some notation: define the space $\mathcal{X}_\nu := \mathbb{R} \times \prod_{i=1}^m \ell^1_{(\nu_i,n)}$ endowed with the norm

$$\left\|\left(\omega, a^1, \ldots, a^m\right)\right\|_{\mathcal{X}_\nu} := \max\left\{|\omega|, \max\left\{\|a^i\|_{(\nu_i,n)} : 1 \leq i \leq m\right\}\right\}.$$

Define projections $\Pi_0 : \mathcal{X}_\nu \to \mathbb{R}$, $\Pi_i : \mathcal{X}_\nu \to \ell^1_{(\nu_i,n)}$, and $\Pi_{i,j} : \mathcal{X}_\nu \to \ell^1_{\nu_i}$ by

$$\Pi_0\left(\omega, a^1, \ldots, a^m\right) := \omega, \quad \Pi_i\left(\omega, a^1, \ldots, a^m\right) := a^i, \quad \Pi_{i,j}\left(\omega, a^1, \ldots, a^m\right) := \left[a^i\right]_j,$$

where $1 \leq i \leq m$, $1 \leq j \leq n$.

Let $N = (N_1, \ldots, N_m) \in \mathbb{N}^m$ be a given collection of truncation parameters and define $\Pi_{N_i} : \ell^1_{(\nu_i,n)} \to \ell^1_{(\nu_i,n)}$, where $1 \leq i \leq m$, by

$$\Pi_{N_i}\left(a^i\right) := \begin{cases} a^i_k, & 0 \leq k \leq N_i - 1, \\ \mathbf{0}_n, & k \geq N_i, \end{cases}$$

and the Galerkin projection $\Pi_N : \mathcal{X}_\nu \to \mathcal{X}_\nu$ by

$$\Pi_N\left(\omega, a^1, \ldots, a^m\right) := \left(\omega, \Pi_{N_1}\left(a^1\right), \ldots, \Pi_{N_m}\left(a^m\right)\right).$$

Henceforth we shall identify $\Pi_N\left(\omega, a^1, \ldots, a^m\right)$ and $\Pi_{N_i}\left(a^i\right)$ with

$$\left[\omega, (a^1_k)_{k=0}^{N_1-1}, \ldots, (a^m_k)_{k=0}^{N_m-1}\right] \in \mathbb{R}^{1+n\sum_{i=1}^m N_i} \qquad \text{and} \qquad \left[a^i_0, \ldots a^i_{N_i-1}\right] \in \mathbb{R}^{nN_i},$$

respectively. This is a slight abuse of notation, but it reduces clutter. It should be clear from the context when to interpret a variable in the finite dimensional space and when to interpret it as an element of an infinite dimensional space with zeros in the tail. Finally, set $\mathcal{X}^N_\nu := \Pi_N\left(\mathcal{X}_\nu\right) \simeq \mathbb{R}^{1+n\sum_{i=1}^m N_i}$.

Definition 2 (Finite dimensional reduction of F)**.** The finite dimensional reduction of F is the map $F_N : \mathcal{X}^N_\nu \to \mathcal{X}^N_\nu$ defined by

$$F_N\left(\left[\omega, (a^1_k)_{k=0}^{N_1-1}, \ldots, (a^m_k)_{k=0}^{N_m-1}\right]\right) := \Pi_N\left(F\left(\omega, a^1, \ldots, a^m\right)\right).$$

3.3 A Newton-like scheme

In this section we introduce a method for proving the existence of an exact zero of F by using an approximate zero of F_N. The main idea is to build a Newton-like scheme in the infinite dimensional setting by using approximate data obtained via numerical simulation. Assume that we have computed the following:

- (**C1**): An approximate zero $\hat{x} \in \mathbb{R}^{1+n\sum_{i=1}^m N_i}$ of F_N, and $\hat{x} = \left(\hat{\omega}, \hat{a}^1, \ldots, \hat{a}^m\right)$, where $\hat{\omega} > 0$.
- (**C2**): An approximate *injective* inverse A_N of $DF_N\left(\hat{x}\right)$.

The finite dimensional data will be used to construct a Newton-like operator T for F such that the zeros of F will correspond to fixed points of T and vice versa.

We start by constructing approximations of $DF\left(\hat{x}\right)$ and its inverse by extending $DF_N\left(\hat{x}\right)$ and A_N to $\mathcal{X}_\nu$ and $\mathcal{X}_{\tilde{\nu}}$, respectively. Recall that $c^i\left(a^i\right)$ decays geometrically to 0 as $k \to \infty$ by (3.4), for any $a^i \in \ell^1_{(\nu_i,n)}$. Moreover, $c^i_k\left(\hat{a}^i\right) = \mathbf{0}_n$ for all $k > N_g\left(N_i - 1\right)$ by (3.3), since $\hat{a}^i_k = \mathbf{0}_n$ for all $k \geq N_i$. Therefore, if the truncation sizes N_i are sufficiently large, and $\max\left\{t_i - t_{i-1} : 1 \leq i \leq m\right\}$ is sufficiently small, the linear part of F corresponding to $\omega k a^i_k$, where $k \geq N_i$, will be dominant at $\hat{x}$. Consequently, one can construct approximations of $DF\left(\hat{x}\right)$ and its inverse by using $DF_N\left(\hat{x}\right)$ and A_N for the finite dimensional part, respectively, and the linear part of the tail of F for the remainder:

Definition 3 (Approximation of $DF\left(\hat{x}\right)$)**.** The approximate derivative $\widehat{A} : \mathcal{X}_\nu \to \mathcal{X}_{\tilde{\nu}}$ of F at $\hat{x}$ is defined by

$$\Pi_0 \widehat{A}\left(x\right) := \Pi_0 DF_N\left(\hat{x}\right)\Pi_N\left(x\right),$$

$$\left(\Pi_i \widehat{A}\left(x\right)\right)_k := \begin{cases} \left(\Pi_i DF_N\left(\hat{x}\right)\Pi_N\left(x\right)\right)_k, & 0 \leq k \leq N_i - 1, \\ \hat{\omega} k \left(\Pi_i\left(x\right)\right)_k, & k \geq N_i, \end{cases},$$

where $1 \leq i \leq m$.

Definition 4 (Approximate inverse of $DF(\hat{x})$)**.** The approximate inverse A of $DF(\hat{x})$ on $\mathcal{X}_{\tilde{\nu}}$ is defined by

$$\Pi_0 A(x) := \Pi_0 A_N \Pi_N(x),$$

$$(\Pi_i A(x))_k := \begin{cases} (\Pi_i A_N \Pi_N(x))_k, & 0 \le k \le N_i - 1, \\ \dfrac{1}{\hat{\omega} k} (\Pi_i(x))_k, & k \ge N_i. \end{cases},$$

where $1 \le i \le m$.

Remark 3. The operator A is injective: suppose $Ax = 0$, then $\Pi_N(x) = 0$, since A_N is assumed, see (**C2**) above, to be injective, and $(\Pi_i(x))_k = 0 \in \mathbb{R}^n$ for all $1 \le i \le m$ and $k \ge N_i$, i.e. $x = 0$.

In analogy to the classical notion of a Newton-operator for a finite dimensional map, we now define an infinite dimensional Newton-like operator for F, based at $\hat{x}$, as follows:

Definition 5 (Newton-like operator for F)**.** The Newton-like operator $T : \mathcal{X}_\nu \to \mathcal{X}_\nu$ for F, based at $\hat{x}$, is defined by

$$T(x) := x - AF(x).$$

An immediate consequence of the fact that A is injective is the following:

Proposition 5. *$T(x) = x$ if and only if $F(x) = 0$.*

If $\hat{x}$ is a sufficiently accurate approximate zero of F, we expect to find an *exact* zero x^* of F, i.e., a fixed point of T, in a small neighborhood of $\hat{x}$. Moreover, if $r > 0$ is sufficiently small (not too small), we anticipate T to be a contraction on $B_r(\hat{x})$. To see why, let $x_1, x_2 \in B_r(0)$, $r > 0$ be arbitrary and consider the following factorization:

$$\begin{aligned} DT(\hat{x} + x_1) x_2 &= (I - ADF(\hat{x} + x_1)) x_2 \\ &= \left(I - A\widehat{A}\right) x_2 - A\left(DF(\hat{x} + x_1) - \widehat{A}\right) x_2. \end{aligned} \tag{3.6}$$

The first term in (3.6) is related to the numerical part of the problem and measures the quality of the approximate inverse A_N, since $I - A\widehat{A}$ vanishes in the tail while the finite dimensional part is the matrix $I_N - A_N DF_N(\hat{x})$. In particular, it is expected to be small by construction. The second term is of a more fundamental nature and involves the analysis of the infinite dimensional operator DF in a neighborhood of the numerical approximation $\hat{x}$. Intuitively, we expect the difference $\left(DF(\hat{x} + x_1) - \widehat{A}\right) x_2$ to be small for small x_1 if $\widehat{A}$ is an accurate approximation of DF near $\hat{x}$. As mentioned before, this is likely to be true if the truncation sizes N_i are sufficiently large, and the mesh-size and radius r are sufficiently small. Altogether, these observations explain why it is plausible for T to be contracting near $\hat{x}$.

The following theorem quantifies the above assertions and is amenable to rigorous numerical analysis. The proof is the same as for the case of a single domain, see [14].

Theorem 1 (Contraction mapping principle with variable radius)**.** *Assume that the following conditions are satisfied:*

(i) There exist bounds $Y_{i,j},\ Z_{i,j}(r) \ge 0$ such that

$$\|\Pi_{i,j}(T(\hat{x}) - \hat{x})\|_{\nu_i} \le Y_{i,j}, \tag{3.7}$$

$$\sup_{x_1, x_2 \in B_r(0)} \|\Pi_{i,j} DT(\hat{x} + x_1) x_2\|_{\nu_i} \le Z_{i,j}(r), \tag{3.8}$$

for all $1 \le i \le m$, $1 \le j \le n$, and bounds $Y_0,\ Z_0(r) \ge 0$ such that

$$|\Pi_0(T(\hat{x}) - \hat{x})| \le Y_0, \tag{3.9}$$

$$\sup_{x_1, x_2 \in B_r(0)} |\Pi_0 DT(\hat{x} + x_1) x_2| \le Z_0(r), \tag{3.10}$$

where $r > 0$.

(*ii*) *There exists a radius* $\hat{r} > 0$ *such that*

$$\max\left\{\max_{1\leq i\leq m, 1\leq j\leq n}\left\{Z_{i,j}\left(\hat{r}\right)+Y_{i,j}\right\},\ Z_0\left(\hat{r}\right)+Y_0\right\}<\hat{r}.$$

Then $T : B_{\hat{r}}\left(\hat{x}\right) \to B_{\hat{r}}\left(\hat{x}\right)$ *is a contraction.*

Remark 4. The Y-bounds measure the accuracy of the approximate solution $\hat{x}$, while the Z-bounds measure the contraction rate of the Newton-like operator T.

The Z-bounds are polynomials in r, as will be shown in section 6.2, which motivates the following terminology:

Definition 6 (Radii-polynomials)**.** The radii-polynomials for T are defined by

$$p_{i,j}\left(r\right) := Z_{i,j}\left(r\right)+Y_{i,j}-r, \quad p_0\left(r\right) := Z_0\left(r\right)+Y_0-r,$$

where $1 \leq i \leq m$, $1 \leq j \leq n$.

Corollary 1. *If* $p_0\left(\hat{r}\right), p_{i,j}\left(\hat{r}\right) < 0$ *for all* $1 \leq i \leq m$ *and* $1 \leq j \leq n$*, where* $\hat{r} > 0$*, then* $T : B_{\hat{r}}\left(\hat{x}\right) \to B_{\hat{r}}\left(\hat{x}\right)$ *is a contraction.*

Note that Corollary 1 also provides a rigorous error-bound for the approximate solution:

Proposition 6. *Suppose* x^* *is the fixed point of* T *in* $B_{\hat{r}}\left(\hat{x}\right)$*, then*

$$\left\|u^*-\hat{u}\right\|_\infty \leq \hat{r}, \quad \left|\omega^*-\hat{\omega}\right| \leq \hat{r},$$

where $u^*, \hat{u} : [0,1] \to \mathbb{R}^n$ *are the exact and approximate periodic orbit with frequency* ω^* *and* $\hat{\omega}$ *defined by* x^* *and* $\hat{x}$*, respectively.*

4 Domain decomposition

In this section we present a procedure, partially based on heuristics, for computing an efficient grid $\mathscr{P}_m$ which facilitates the rigorous validation process. The main idea is to compute a grid for which the decay rates of the coefficients $\hat{a}^i$ are sufficiently high and *uniformly distributed* over the subdomains. The motivation for this choice is based on the observation that a combination of high-decay rates (uniformly distributed) and a relatively small number of modes will help to control the tail estimates in Lemma 6 on each subdomain in a uniform way. In turn, this will aid in verifying that T is a contraction.

4.1 A heuristic procedure for computing $\mathscr{P}_m$

In this section we introduce a heuristic procedure for computing a grid $\mathscr{P}_m$ such that the decay rate of the Chebyshev coefficients $\left[\hat{a}^i\right]_j$, where $1 \leq j \leq n$, is the same on each subdomain. The main idea is to construct $\mathscr{P}_m$ by using the Bernstein ellipses introduced in Proposition 1. Suppose $u^* : [0,1] \to \mathbb{R}^n$ is the exact solution of the ODE under consideration (assuming it exists). Furthermore, assume that the obstructions for analytically extending the components $\left[u^*\right]_j$ to the entire complex plane are the presence of poles $\{z_{k,j}\}_{k=1}^{N_{p,j}}$.

Write $u_i^* := u^*|_{[t_{i-1},t_i]}$ and observe that the Bernstein ellipse associated to the map

$$t \mapsto \left[u_i^*\left(\frac{t_i-t_{i-1}}{2}\left(t+1\right)+t_{i-1}\right)\right]_j, \tag{4.1}$$

where $t \in [-1,1]$, i.e., the largest ellipse with foci -1 and 1 to which the latter map can be analytically extended, has the following measurements: its linear eccentricity is equal to 1, the length of the semi-major axis is equal to

$$P_j\left(t_{i-1},t_i\right) := \min_{1\leq k\leq N_{p,j}} \frac{\left|z_{k,j}-t_{i-1}\right|+\left|z_{k,j}-t_i\right|}{t_i-t_{i-1}}, \tag{4.2}$$

and the length of the semi-minor axis is equal to $\sqrt{P_j\left(t_{i-1},t_i\right)^2-1}$. Therefore, the decay rate of the Chebyshev coefficients of $[u_i^*]_j$ is given by

$$P_j\left(t_{i-1},t_i\right)+\sqrt{P_j\left(t_{i-1},t_i\right)^2-1}, \tag{4.3}$$

due to Proposition 1. We shall refer to the latter quantity as the size of the Bernstein ellipse of $[u_i^*]_j$. Note that if the components of the vector field are all coupled, the components of u^* will (generically) have the same poles. In this case the decay rate (4.3) will be the same for all $1 \leq j \leq n$.

Set $P\left(t_i,t_{i-1}\right) := \min_{1\leq j\leq n} P_j\left(t_{i-1},t_i\right)$ and note that the smallest Bernstein ellipse of the components of u_i^* has size

$$\nu_e := P\left(t_{i-1},t_i\right)+\sqrt{P\left(t_{i-1},t_i\right)^2-1}. \tag{4.4}$$

Hence, equidistributing decay rates of $\hat{a}^i$ corresponds to equidistributing $P(t_{i-1},t_i)$. Next, define $\Phi_m : \mathscr{G}_m \subset \mathbb{R}^{m-1} \to \mathbb{R}^{m-1}$ by

$$\Phi_m\left(t_1,\ldots,t_{m-1}\right) := \begin{pmatrix} P\left(t_0,t_1\right)-P\left(t_1,t_2\right) \\ \vdots \\ P\left(t_{m-2},t_{m-1}\right)-P\left(t_{m-1},t_m\right) \end{pmatrix},$$

where $\mathscr{G}_m := \left\{\left(t_1,\ldots,t_{m-1}\right)\in\mathbb{R}^{m-1} : 0<t_1<\ldots<t_{m-1}<1\right\}$, and observe that the zeros of Φ_m characterize the grids which equidistribute (4.4) over the subdomains $[t_{i-1},t_i]$. Therefore, the desired grid can be obtained by computing a zero of Φ_m.

We shall approximate a zero of Φ_m by using Newton's method. In order for Newton's method to be successful, however, we need to supply a sufficiently accurate initial guess for a zero of Φ_m. To find such an initial guess, we interpret Φ_m as a smooth vector field on $\mathscr{G}_m$, and the desired grid as a steady state of the associated dynamical system. This interpretation makes sense, since $\mathscr{G}_m$ is invariant under the flow induced by Φ_m, i.e., the ordering of the grid points $0<t_1<\ldots<t_{m-1}<1$ is preserved under the flow. The reason for this is that successive grid points t_{i-1}, t_i *repel* each other whenever their mutual distance is sufficiently small due to the factors $\frac{\pm 1}{t_i-t_{i-1}}$ in $[\Phi_m\left(t_1,\ldots,t_{m-1}\right)]_{i-1}$ and $[\Phi_m\left(t_1,\ldots,t_{m-1}\right)]_i$, see (4.2).

If $\mathscr{G}_m$ contains a stable equilibrium of Φ_m, one can approximate its location, i.e., compute an initial guess for the desired grid, by integrating the ODE

$$\frac{\mathrm{d}t}{\mathrm{d}\tau} = \Phi_m\left(t\right), \quad \tau\in[0,\tau_0], \tag{4.5}$$

for sufficiently large $\tau_0>0$. In practice, we start with a uniformly distributed grid and follow the flow of (4.5) for some time. In all our numerical experiments this process appeared to converge to an equilibrium state and yielded a sufficiently accurate initial guess for initiating Newton's method.

4.2 Approximation of the complex singularities

In the previous section we explained how to compute grids by computing zeros of Φ_m. In order to construct the map Φ_m, however, one needs to determine the complex singularities of the exact solution u^*. In this section we outline some of the algorithmic aspects for approximating the relevant complex singularities of u^*, i.e., the ones which determine the sizes of the Bernstein ellipses, by using an approximate solution of the ODE and the rational interpolation scheme developed in [26, 27].

The main idea in [26, 27] is as follows: given an analytic function $f : [a,b] \to \mathbb{R}$ approximate its analytic extension into the complex plane by constructing a rational interpolant $\frac{p}{q}$. This is accomplished by sampling f at the Chebyshev points in $[a,b]$ and solving (if necessary in a least square sense) the problem

$$p\left(y_j\right) - f\left(y_j\right)q\left(y_j\right) = 0, \quad 0\leq j\leq K, \tag{4.6}$$

where $(y_j)_{j=0}^K$ are the Chebyshev points on $[a,b]$, $K \in \mathbb{N}$, and p, q are polynomials of degree N_p, N_q, respectively. This will yield a rational interpolant $\frac{p}{q}$, provided $q(y_j) \neq 0$ for all $0 \leq j \leq K$. The associated rational interpolant is referred to as a rational interpolant of type (N_p, N_q). The complex singularities of f can be approximated by computing the roots of q. The degrees of p and q, however, should be chosen carefully in order to avoid spurious poles. To reduce the number of spurious poles, the algorithm in [26,27] uses heuristics to determine whether the prescribed degree for q was not too large and lowers it if necessary.

Let $\tilde{u} = \sum_{i=1}^{\tilde{m}} \mathbf{1}_{[\tilde{t}_{i-1},\tilde{t}_i]} \tilde{u}_i$ be an approximate solution of the ODE, where $\tilde{u}_i = \tilde{a}_0^i + 2\sum_{k=1}^{\tilde{N}_i - 1} \tilde{a}_k^i T_k^i$ and $\left(\tilde{t}_i\right)_{i=0}^{\tilde{m}}$ is a partition of $[0,1]$. The idea is to use $\tilde{u}$ to approximate the complex singularities of the (true) solution u^*, namely by constructing rational interpolants for each $[\tilde{u}_i]_j$. Consider any $1 \leq i \leq m$, $1 \leq j \leq n$, and initialize $N_q = 1$. Then follow the procedure as described below:

1. Compute an approximate rational interpolant for $[u_i^*]_j$ of type $\left(\left\lfloor \frac{2\tilde{N}_i}{3} \right\rfloor, N_q\right)$ with $K = \left\lfloor \frac{2\tilde{N}_i}{3} \right\rfloor + N_q$ by using the approximate solution $[\tilde{u}_i]_j$. The specific choices for the parameters are motivated in Remark 5.

2. Compute the absolute value, denoted by Δ, of the difference of the approximate size of the Bernstein ellipse of $[u_i^*]_j$ and the decay rate of $\left[\tilde{a}^i\right]_j$. The decay rate of $\left[\tilde{a}^i\right]_j$ is estimated by using the least-square method to find the best line through the data points

$$\left\{\left(k, \log\left|\left[\tilde{a}_k^i\right]_j\right|\right) : 1 \leq k \leq \tilde{N}_i - 1, \left|\left[\tilde{a}_k^i\right]_j\right| > 10^{-16}\right\}.$$

   The decay rate is then approximated by e^{-s}, where s is the slope of this line. In particular, $\Delta = |\nu_e - e^{-s}|$, where ν_e is defined in (4.4).

3. If $\Delta < 0.05$, then the approximation of the relevant singularities is deemed sufficiently accurate and we terminate the procedure. Otherwise, if $N_q < \left\lfloor \frac{\tilde{N}_i}{3} \right\rfloor$, we increase N_q by one and return to step 1. If $N_q = \left\lfloor \frac{\tilde{N}_i}{3} \right\rfloor$, the approximation of the singularities was unsuccessful and the program is terminated. The significance of Δ and the specific choice for the tolerance and stopping criteria are explained in Remark 6.

Remark 5. The value for K in step 1 is the smallest value for which (4.6) is guaranteed to admit an exact solution. The motivation for choosing $N_p = \left\lfloor \frac{2\tilde{N}_i}{3} \right\rfloor$ is that if one expects the existence of complex singularities (which we generally do) one should choose $N_p < \tilde{N}_i - 1$, since the rational interpolation scheme would yield $p = [\tilde{u}_i]_j$ and $q \equiv 1$ for $N_p \geq \tilde{N}_i - 1$. At the same time, N_p should be chosen sufficiently large in order for the rational interpolant to be an accurate approximation of $[u_i^*]_j$. The specific choice $N_p = \left\lfloor \frac{2\tilde{N}_i}{3} \right\rfloor$ is based on experimentation and the suggestions in [35].

Remark 6. The quantity Δ defined in step 2 is used to asses the accuracy of the approximation of the relevant singularities. Indeed, if the approximation of the relevant singularities is accurate, then Δ should be relatively small by Proposition 1. In practice, Δ varied at best between 0.01 and 0.05 which motivated the choice for the tolerance in step 3. Furthermore, the rational interpolants were constructed by using approximate solutions $\tilde{u}$ defined on relatively fine grids with high decay on each subdomain. Hence we expected a relatively small number of complex singularities per subdomain. This motivated the choice for the stopping criterion $N_q = \left\lfloor \frac{\tilde{N}_i}{3} \right\rfloor$.

5 Applications: periodic and heteroclinic orbits in the Lorenz system

In this section we demonstrate the effectiveness of domain decomposition by using the proposed method to validate periodic and heteroclinic orbits in the Lorenz system which we were not able to validate without decomposition of the domain. In Section 5.2 we consider the validation of a periodic orbit on the Lorenz attractor for which the procedure in Section 3 is directly applicable.

In Section 5.3 we consider a family of periodic orbits near a homoclinic orbit and in Section 5.4 we validate a heteroclinic orbit. In the the latter two cases the procedure in Section 3 cannot be applied directly and needs some modifications, illustrating both the limitations and the flexibility of the method.

5.1 Main algorithm

First we describe the main procedure used for validating solutions of (1.1):

1. Compute an approximate zero $\tilde{x}$ of F with respect to some grid $\left(\tilde{t}_i\right)_{i=0}^{\tilde{m}}$ and approximate the complex singularities of u^* (the exact solution of the ODE) as described in Section 4.2.

2. Choose the number of domains m and use the procedure in Section 4.1 to determine a grid $(t_i)_{i=0}^{m}$ with uniform decay on each subdomain. The number of domains m needs to be chosen in such a way that $\max\{t_i - t_{i-1} : 1 \leq i \leq m\}$ is sufficiently small and the number of modes N_i, as determined below, is sufficiently large. In practice, we chose m by experimentation (see Section 5.2 for an example in which we validated a periodic orbit for different m).

3. Construct an approximate solution $\hat{x}$ on the new grid $(t_i)_{i=0}^{m}$. The number of modes N_i on each subdomain $[t_{i-1}, t_i]$ is chosen in such a way that $\left|\hat{a}_k^i\right|_\infty < 10^{-16}$ for $k \geq N_i$.

4. Determine weights $(\nu_i)_{i=1}^{m}$ for which validation is feasible. We have chosen to fix one weight $\nu > 1$ and set $\nu_i = \nu$ for all $1 \leq i \leq m$, since by construction the decay-rates are the same on all subdomains. Furthermore, ν is determined by first computing an initial guess ν_0, as explained in Remark 7 below, and checking whether validation is feasible with $\nu = \nu_0$. This is accomplished by computing the Y and Z-bounds as defined in Section 6 and constructing the radii-polynomials (without interval arithmetic). Subsequently, we try to determine an interval on which *all* the radii-polynomials are negative. If we do not find such an interval (i.e. validation is not feasible), then we keep decreasing ν (as long as $\nu > 1$) until validation is feasible.

5. Construct the radii-polynomials *with* interval arithmetic and determine an interval $I_{m,\nu}$ at which they are all negative.

Remark 7. The initial guess ν_0 in step 3 is determined by a heuristic procedure that is based on analyzing the bounds $Y_{i,j}$ as stated in Proposition 7 in Section 6. The idea is to choose $\nu_0 > 1$ such that

$$\frac{t_i - t_{i-1}}{2\hat{\omega}} \sum_{k=N_i}^{N_g(N_i-1)+1} \left|\left[c_{k-1}^i(\hat{a}) - c_{k+1}^i(\hat{a})\right]_j\right| \frac{\nu_0^k}{k} \leq \epsilon, \quad \text{for all } 1 \leq i \leq m,\ 1 \leq j \leq n,$$

where $\epsilon > 0$ is a prescribed tolerance which we set equal to 10^{-14} in our algorithm. A rather rough estimation yields

$$\frac{t_i - t_{i-1}}{2\hat{\omega}} \sum_{k=N_i}^{N_g(N_i-1)+1} \left|\left[c_{k-1}^i(\hat{a}) - c_{k+1}^i(\hat{a})\right]_j\right| \frac{\nu_0^k}{k} < \frac{h\nu_0}{\hat{\omega} N_i} \sum_{k=N_i-1}^{N_g(N_i-1)+2} \left|\left[c_k^i(\hat{a})\right]_j\right| \nu_0^k, \tag{5.1}$$

where $h := \max\{t_i - t_{i-1} : 1 \leq i \leq m\}$. Note that $\left[\hat{a}_k^i\right]_j$ and $\left[c_k^i(\hat{a})\right]_j$ are both of order $\mathcal{O}\left(\nu_e^{-k}\right)$, where ν_e, see (4.4), is known by construction of the grid. Therefore, assuming that $\left|\hat{a}_0^i\right|_\infty$ is roughly of the same order on all subdomains, we anticipate that the number of modes per subdomain will be fairly uniformly distributed, say $N_i \approx \bar{N}$, where $\bar{N}$ is the (rounded) average number of modes per subdomain. Altogether, we expect the quantity

$$\frac{h\nu_e}{\hat{\omega}\bar{N}} \sum_{k=\bar{N}-1}^{N_g\left(\bar{N}-1\right)+2} \left(\frac{\nu_0}{\nu_e}\right)^k = \frac{h\nu_e}{\hat{\omega}\bar{N}\left(1 - \frac{\nu_0}{\nu_e}\right)} \left(\left(\frac{\nu_0}{\nu_e}\right)^{\bar{N}} - \left(\frac{\nu_0}{\nu_e}\right)^{N_g\left(\bar{N}-1\right)+3}\right) \tag{5.2}$$

to provide a reasonable estimate for the order of magnitude of (5.1). Moreover, since we need to choose $\nu_0 < \nu_e$ and $\bar{N}$ is relatively small compared to $N_g\left(\bar{N}-1\right)+3$, one can approximate (5.2) by

$$\frac{h\nu_e}{\hat{\omega}\bar{N}\left(1-\frac{\nu_0}{\nu_e}\right)}\left(\frac{\nu_0}{\nu_e}\right)^{\bar{N}}.$$

Hence we have chosen to determine ν_0 by setting the latter quantity equal to ϵ.

5.2 Periodic orbit on the Lorenz-attractor

We have successfully applied our method to validate a periodic orbit of period $L \approx 25.0271$ in the Lorenz system for the classical parameter values. We remark that validation was not feasible without decomposition of the domain. More precisely, the procedure described in Section 5.1 failed for $m = 1$, i.e., with a single domain. The main obstruction to using just one domain was the need for a large number of modes to accurately approximate the orbit, which caused the bounds related to the tail of the Chebyshev approximation to be (too) large. We should mention that it is feasible to validate this periodic orbit using a Fourier basis (and hence a single domain) via the method in [19]. However, Fourier series can be used for problems with periodic boundary conditions only. Furthermore, the number of Fourier modes needed is comparable to the total number of modes in our domain decomposition method, and the latter is readily amenable to general (non-periodic) boundary conditions.

We have reported the computational results in Table 5.1. As expected, the size of the Bernstein-ellipses ν_e (as defined in (4.4)) increases and the (rounded) average number of modes $\bar{N}$ decreases, whenever the number of subdomains m is increased. Moreover, as long as the decrease of $\bar{N}$ outweighs the increase of m, the dimension of X_ν^N decreases, thereby making the proof computationally more efficient. In particular, $m = 34$ was the computationally most efficient choice. We remark, however, that no attempt was made to optimize $\dim \mathcal{X}_\nu^N$ for fixed m. It may be possible to validate the orbit by using a significantly smaller number of modes N_i per subdomain, i.e., by relaxing the requirement that $\left|a_k^i\right|_\infty < 10^{-16}$ for $k \geq N_i$. Finally, for each m the initial guess ν_0 for ν was slightly too large and was lowered by 0.01 in order to make validation feasible.

The approximations of the complex singularities of the orbit are shown in Figure 5.1. Note that the relevant singularities, i.e., the ones which determine the size of the smallest Bernstein ellipse, were fairly uniformly distributed. As a consequence, the resulting grids look close to uniform at first glance, as can be seen in Figure 5.2a. However, we stress that our method for distributing the grid points based on the location of the complex singularities significantly improves the computational efficiency compared to choosing a uniform grid. To illustrate this, notice the dramatic decrease in the dimension of X_ν^N as we proceed from $m = 33$ to $m = 34$, i.e., we add *one* grid point. This is caused by a very subtle redistribution of the grid-points, as shown in Figure 5.2a, which resulted in a relatively large increase in the decay-rates from 1.68 to 1.87, see Table 5.1.

Indeed, at first sight the grids appear to be very similar and it is unclear how the decay-rates could have increased that much. To get some insight, we have depicted two seemingly similar subdomains $[t_{32}, 1]$ and $[\tau_{33}, 1]$ in Figure 5.2b, where $(t_i)_{i=0}^{33}$ and $(\tau_i)_{i=0}^{34}$ denote the grid-points for $m = 33$ and $m = 34$, respectively. The grid-points t_{32} and τ_{33} are so close to each other that the sizes of the Bernstein ellipses associated to $[t_{32}, 1]$ and $[\tau_{33}, 1]$ are determined by the same pair of complex singularities. Nevertheless, the subtle movement of τ_{33} to the right was sufficient to cause the observed increase in the decay-rates. To see this, recall that the computation of the size of the Bernstein ellipses involves a rescaling to $[-1, 1]$, as explained in Section 4.1. This rescaling contributes to the increase in the decay-rates. We note that in other regions in the grid, the redistribution of the grid points (when adding a grid point) leads to a change in which pole determines the size of the Bernstein-ellipse (for some domain). The combination of delicate shifts of all the grid points together leads to the major improvement in the (uniform) decay rate.

The results highlight the effectiveness of the proposed method for performing domain decomposition: the global improvement of the decay-rates due to the subtle repositioning of the grid-points could not have been achieved by merely using uniform grids.

m	$\bar{N}$	$\dim \mathcal{X}_\nu^N$	ν	ν_e	$I_{m,\nu}$
32	79	7618	1.1148	1.6413	$[4.5581 \cdot 10^{-10},\ 1.0217 \cdot 10^{-7}]$
33	76	7498	1.1278	1.6837	$[3.1192 \cdot 10^{-10},\ 1.5371 \cdot 10^{-7}]$
34	63	6433	1.1432	1.8749	$[3.8158 \cdot 10^{-10},\ 1.1950 \cdot 10^{-7}]$
35	61	6457	1.1529	1.9056	$[3.3529 \cdot 10^{-10},\ 1.0320 \cdot 10^{-7}]$
36	61	6610	1.1564	1.9115	$[3.1282 \cdot 10^{-10},\ 1.1097 \cdot 10^{-7}]$

Table 5.1: Numerical results for a validated periodic orbit of period $L \approx 25.0271$ in the classical Lorenz system. In each case the number of modes N_i per domain was approximately the same. The number $\bar{N}$ denotes the (rounded) average number of modes per domain.

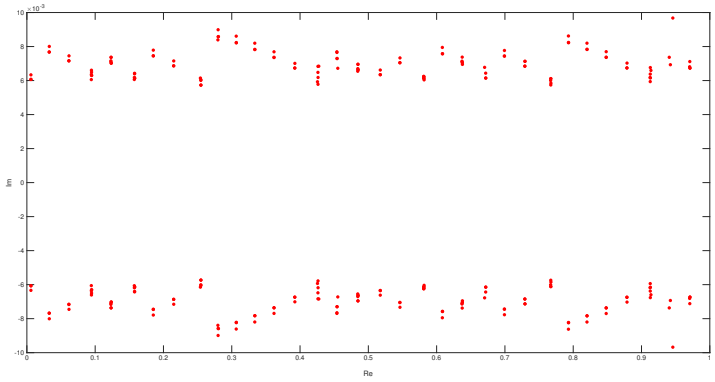

Figure 5.1: The approximate complex singularities of the validated periodic orbit. The complex singularities were computed with the procedure described in Section 4.2.

5.3 Family of periodic orbits near a homoclinic connection

In this section we will validate periodic orbits close to the homoclinic orbit to the origin as $\rho \downarrow \rho_{\text{hom}} \approx 13.926557407$. The map F as defined in definition 1, however, has to be slightly adapted to accomplish this goal. The reason F has to be adapted can be seen in Figure 5.3, which depicts the dependency of L on ρ. In particular, note that the bifurcation curve is almost vertical near ρ_{hom}. Therefore, $DF_N(\hat{x})$ is close to singular near the critical parameter value ρ_{hom}. Consequently, the approximate inverse A_N of $DF_N(\hat{x})$ is badly conditioned near ρ_{hom}, which causes the estimates in Proposition 8 to blow up, which in turn will obstruct the validation process.

The latter problem can be solved by adding an additional equation to F and including the parameter ρ as an additional variable to solve for. We adapt the method in Section 3 as follows:

- Include ρ as an additional variable in $\mathcal{X}_\nu$, i.e., set $\mathcal{X}_\nu := \mathbb{R} \times \mathbb{R} \times \prod_{i=1}^m \ell^1_{(\nu_i,n)}$ and write $x = \left(\rho, \omega, a^1, \ldots, a^m\right) \in \mathcal{X}_\nu$.
- Define the norm and projections on $\mathcal{X}_\nu$ in the same way as before by including an additional projection $\Pi_{-1} : \mathcal{X}_\nu \to \mathbb{R}$ onto the parameter space defined by $\Pi_{-1}\left(\rho, \omega, a^1, \ldots, a^m\right) := \rho$.
- Define $\widetilde{F} : \mathcal{X}_\nu \to \mathcal{X}_{\tilde{\nu}}$ by

  $$\widetilde{F}(x) := \left(f_{-1}(\rho, \omega, a_1, \ldots, a_m), f_0(a^1), f_1(\rho, \omega, a^1, a^m), f_2(\rho, \omega, a^1, a^2), \ldots f_m(\rho, \omega, a^{m-1}, a^m)\right),$$

  where $f_0, \ldots, f_m$ are defined as before, and we choose

  $$f_{-1} := \langle V_0, \Pi_N(x) - U_0 \rangle$$

  where V_0 is approximately tangent to the solution curve $(\rho, \phi(\rho))$ of F_N, and U_0 is a "predictor" for the next point on the solution curve.

The corresponding modifications to the bounds Y and Z are described in Section 6.3.1.

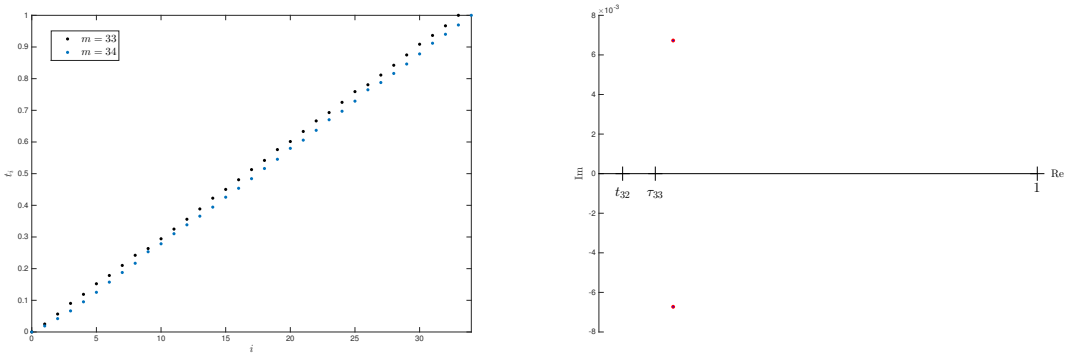

(a) (b)

Figure 5.2: (a) A plot of the two grids $(i, t_i)_{i=0}^{33}$ and $(i, \tau_i)_{i=0}^{34}$ corresponding to $m = 33$ and $m = 34$, respectively. (b) A plot of the grid-points t_{32}, τ_{33} and the complex singularities (colored in red) which determine the size of the Bernstein ellipses associated to $[t_{32}, 1]$ and $[\tau_{33}, 1]$.

5.3.1 Results

To examine the performance of the proposed method we first determined how far we could push the period by using only one domain. Next, we extended the result by using domain decomposition. In particular, we validated a long periodic orbit of period $L \approx 100.2254$ which revealed a limitation of the proposed method. In fact, there the standard algorithm breaks down in two spots.

First, it was not feasible to determine a grid by using the procedure in Section 4, since in the region where the orbit is flat (i.e. near the equilibrium at the origin in phase space, see Figure 1.3) we were not able to compute accurate approximations of the complex singularities. A likely reason for this is that the complex singularities in this region are located too far away from the real axis (i.e. there are no "nearby" poles).

Second, after fixing the grid in the flat part of the solution in an ad-hoc manner (discussed below), the number of modes N_i in this part of the grid, as determined via the procedure in Section 5.1, was very small. To see why the use of such a small number of modes is an obstruction, recall that the approximate inverse A, as defined in definition 4, was constructed under the assumption that $\omega k a_k^i$ is the dominant term in $\left(f_i\left(\omega, a^{i-1}, a^i\right)\right)_k$ for $k \geq N_i$ in a small neighborhood of the numerical approximation. The latter assumption, however, is only satisfied if the truncation dimensions N_i are sufficiently large and $\max\{t_i - t_{i-1} : 1 \leq i \leq m\}$ is sufficiently small (see definition 1). Consequently, in order to validate the flat part of the orbit (where a small number of modes per subdomain is used), one needs to ensure that the grid is sufficiently fine there.

To validate the long periodic orbit we constructed a grid which was uniform in the region where the orbit is flat, and outside this region (where the number of modes per subdomain were relatively large) the grid-points were placed by using the complex singularities as described in Section 4. We remark that another strategy for resolving the above issue is to use only one domain for the flat part of the orbit, and to artificially increase the number of modes on this subdomain by padding with zeros. We have succeeded in validating the orbit in this way as well. The results are reported in Table 5.2. In particular, in the case $m = 7$ we used one subdomain with 1800 modes (of which only the first 136 were nonzero) to approximate the flat part of the orbit. In the case $m = 506$ we used 500 equally spaced subdomains each using (on average) about five modes to represent the flat part of the orbit.

By adapting the algorithm, we are thus able to validate very long orbits near the homoclinic connection. We conclude this section by remarking on two possible improvements to the domain decomposition technique.

Remark 8. The results show that the proposed method is not directly applicable for validating orbits which exhibit slow-fast behavior on different time-scales. In this particular case, a more effective approach for validating the long periodic orbit would be to avoid "numerical integration" of the slow passage and to analyze the (relatively simple) dynamics near the equilibrium by other

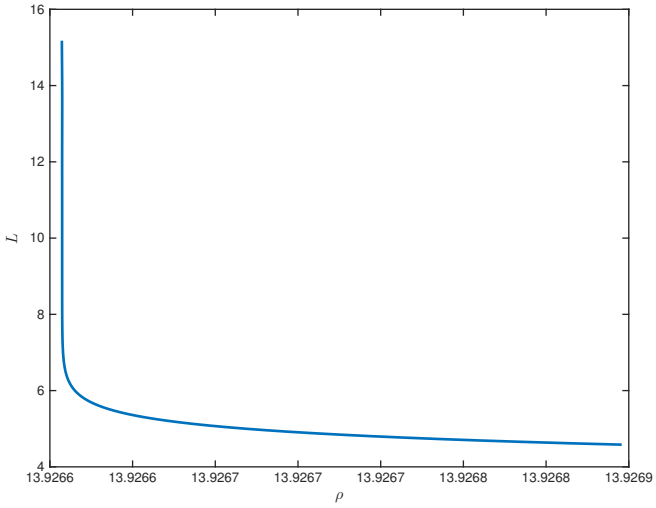

Figure 5.3: The dependence of the period L as a function of ρ obtained via non-rigorous pseudo-arclength continuation.

L	m	$\dim \mathcal{X}_\nu^N$	$I_{m,\nu}$
4.5473	1	566	$\left[4.4568 \cdot 10^{-11},\ 8.4403 \cdot 10^{-6}\right]$
100.2554	7	5894	$\left[1.5186 \cdot 10^{-11},\ 7.4915 \cdot 10^{-8}\right]$
100.2554	506	8441	$\left[1.5174 \cdot 10^{-11},\ 4.2914 \cdot 10^{-6}\right]$

Table 5.2: Numerical results for two periodic orbits near the homoclinic connection. The periodic orbit of period $L \approx 100.2554$ was in both cases validated on a grid for which (the same) six subdomains were used to approximate the non-flat part of the orbit.

means (normal forms, lambda lemma, etc.).

Remark 9. For this particular problem, distribution of the grid-points based on the location of the complex singularities is not an efficient choice, since our domain decomposition algorithm will concentrate most of the grid-points outside the region where the orbit is flat. Indeed, (in general) our domain decomposition algorithm will yield relatively large subdomains in regions where the complex singularities are located far away from the real-axis. This can obstruct the validation process as $\max\{t_i - t_{i-1} : 1 \leq i \leq m\}$ might be too large. To resolve this issue, one can try to improve the domain decomposition algorithm by incorporating constraints on the maximal distance between successive grid-points.

5.4 Heteroclinic orbit

To show that our method is applicable to more general BVPs than just periodic boundary conditions, we consider the validation of a transverse heteroclinic orbit from $q^+ = (\sqrt{\beta(\rho-1)}, \sqrt{\beta(\rho-1)}, \rho-1)$ to the origin for the classical parameter values in the Lorenz system. Both the origin and q^+ are hyperbolic, and $\dim(W^s(\mathbf{0})) = \dim(W^u(q^+)) = 2$. In particular, the *transversality* condition $n_u + n_s = n + 1$, where $n_u = \dim(W^u(q^+))$, $n_s = \dim(W^s(\mathbf{0}))$, is satisfied.

The idea is to set up a suitable BVP which characterizes the heteroclinic orbit, and to adjust the method in Section 3 accordingly in order to solve the BVP. A heteroclinic orbit from q^+ to the

origin is characterized by

$$\begin{cases} \dfrac{du}{dt} = Lg\left(u\right), & t \in [0,1], \\ u(0) = P\left(\alpha\right), & \alpha \in V_u, \\ u(1) = Q\left(\phi\right), & \phi \in V_s, \end{cases} \tag{5.3}$$

where $L > 0$ is a *fixed* integration time and $P : V_u \subset \mathbb{R}^2 \to W^u_{loc}\left(q^+\right)$, $Q : V_s \subset \mathbb{R}^2 \to W^s_{loc}\left(\mathbf{0}\right)$ are local parameterizations of $W^u_{loc}\left(q^+\right)$ and $W^s_{loc}\left(\mathbf{0}\right)$, respectively. We have used the parameterization method developed in [11, 22, 33] to explicitly compute P and Q.

The idea of the computational method developed in [11, 22, 33] is to construct P by expanding it as a power series, and by requiring that it conjugates the unstable part of the linearized dynamics around the origin with the dynamics on $W^u_{loc}\left(q^+\right)$. The parameterization Q is obtained similarly. The method yields approximate parameterizations P_{N_u} and Q_{N_s}, where $N_s, N_u \in \mathbb{N}$ are the degrees up to which the power series are computed, and establishes the existence of exact parameterizations P and Q via a rigorous numerical scheme. In particular, the procedure provides rigorous error bounds $\delta_u, \delta_s > 0$ such that

$$\left\|P - P_{N_u}\right\|_\infty \leq \delta_u, \quad \left\|Q - Q_{N_s}\right\|_\infty \leq \delta_s.$$

Since heteroclinic orbits are invariant under translations in time, we need to introduce a phase condition to remove this extra degree of freedom. This can be accomplished by, roughly speaking, restricting P or Q to a domain of one dimension less. We have used the same phase condition as in [22]: let $\Theta_\mu : \mathbb{S}^1 \to V_s$ be the embedding of the unit circle into V_s defined by

$$\Theta_\mu\left(\phi\right) := \mu\left(\cos\phi, \sin\phi\right),$$

where $\mu > 0$ is sufficiently small, and consider the following equivalent formulation of (5.3):

$$\begin{cases} \dfrac{du}{dt} = Lg\left(u\right), & t \in [0,1], \\ u(0) = P\left(\alpha\right), & \alpha \in V_u, \\ u(1) = Q \circ \Theta_\mu\left(\phi\right), & \phi \in V_s. \end{cases} \tag{5.4}$$

The procedure in Section 3, however, needs to be modified before it can be applied to (5.4). First, note that we fix the integration time L. Furthermore, the parameterization variables ϕ and α have to be treated as unknown variables. Therefore, in order to solve (5.4) we modify the procedure in Section 3 as follows:

- Set $\mathcal{X}_\nu := \mathbb{S}^1 \times V_u \times \prod_{i=1}^m \ell^1_{(\nu_i, n)}$ and write $x = \left(\phi, \alpha, a^1, \ldots, a^m\right)$.
- Adapt the set-up described in Section 3.2 by replacing Π_0 with projections $\Pi_{0,j} : \mathcal{X}_\nu \to \mathbb{R}$, where $1 \leq j \leq 3$, defined by

  $$\Pi_{0,1}\left(\phi, \alpha, a^1, \ldots, a^m\right) := \phi, \quad \Pi_{0,j}\left(\phi, \alpha, a^1, \ldots, a^m\right) = \left[\alpha\right]_{j-1},$$

  for $j \in \{2, 3\}$.
- Define $F : \mathcal{X}_\nu \to \mathbb{R}^3 \times \prod_{i=1}^m \ell^1_{(\tilde{\nu}_i, n)}$ analogously as in definition 1 by incorporating the modified boundary conditions into f_0 and $(f_1)_0$:

  $$F\left(x\right) := \left(f_0\left(\phi, a^m\right), f_1\left(\alpha, a^1\right), f_2\left(a^1, a^2\right), \ldots, f_m\left(a^{m-1}, a^m\right)\right),$$

  where

  $$f_0\left(\phi, a^m\right) := a^m_0 + 2\sum_{k=1}^\infty a^m_k - Q \circ \Theta_\mu\left(\phi\right),$$

  $$\left(\Pi_1 F\left(x\right)\right)_0 = a^1_0 + 2\sum_{k=1}^\infty \left(-1\right)^k a^1_k - P\left(\alpha\right),$$

  $$\left(\Pi_i F\left(x\right)\right)_k = k a^i_k - \frac{L\left(t_i - t_{i-1}\right)}{4}\left(c^i_{k-1} - c^i_{k+1}\right), \quad k \in \mathbb{N},\ 1 \leq i \leq m.$$

m	$\bar{N}$	$\dim \Pi_N(\mathcal{X}_\nu)$	ν	$I_{m,\nu}$
55	42	6864	1.3710	$\left[6.4412 \cdot 10^{-9},\ r^*\right]$

Table 5.3: Numerical results for the connecting orbit from q^+ to the origin. The interval $I_{m,\nu}$ is the set of admissible radii on which the radii-polynomials were proven to be strictly negative.

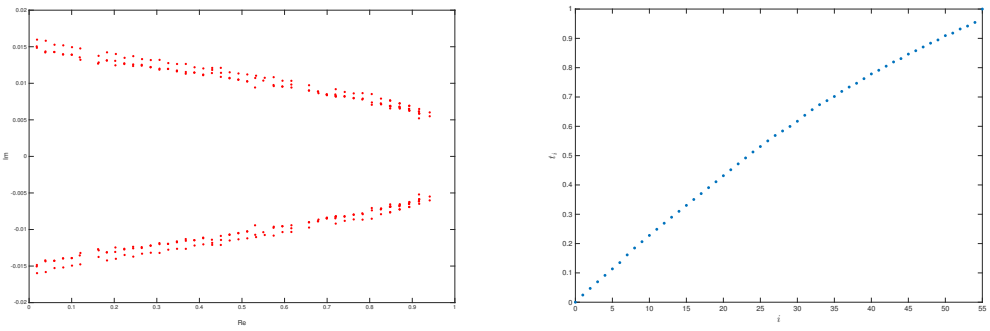

(a) (b)

Figure 5.4: (a) The complex singularities of the connecting orbit. (b) The grid, determined by the algorithm in Section 4, on which the connecting orbit was validated.

- Define the finite dimensional reduction $F_N : \mathbb{R}^{n\left(1+\sum_{i=1}^m N_i\right)} \to \mathbb{R}^{n\left(1+\sum_{i=1}^m N_i\right)}$ of F by $F_N(x) := \Pi_N F(x)$, and by replacing P, Q with P_{N_u}, Q_{N_s}, respectively.
- Define A and $\widehat{A}$ as before without the factors $\dfrac{1}{\hat{\omega}}$ and $\hat{\omega}$, respectively.

The corresponding modifications to the estimates Y and Z are described in Section 6.3.2.

5.4.1 Results

We have successfully validated a connecting orbit from q^+ to the origin by using the procedure described in Section 5.1. The integration time was $L = 30$. The parameters used for approximating the stable and unstable manifolds were $N_u = 15$, $N_s = 25$, $\mu = 0.4$, and $r^* = 10^{-6}$. The meaning of r^* is explained in Section 6.3.2. The corresponding error-bounds for the parameterizations were $\delta_u \leq 4.6847 \cdot 10^{-12}$ and $\delta_s \leq 5.9717 \cdot 10^{-15}$. We have kept the size of $W^u_{loc}(q^+)$ small so that the orbit was relatively "long" and sufficiently complicated to test the domain decomposition method. The computational results are reported in Table 5.3.

The complex singularities and the corresponding grid are shown in Figures 5.4a and 5.4b, respectively. Figure 5.4a shows that the complex singularities move closer to the real axis as the orbit spirals away from q^+ up until the point at which the orbit travels to the origin in (roughly) a straight line in phase space (see Figure 1.1). In this last part of the orbit there appear to be no complex singularities close to the real-axis. These observations are reflected in the distribution of the grid-points as shown in Figure 5.4b: the distance between successive grid-points decreases as the orbit spirals away from q^+, except for the distance between the second to last grid point and the last one, which is substantially larger.

6 The estimates need to prove contraction

In this section we give explicit expression for the bounds Y and Z in Theorem 1. We focus primarily on periodic boundary conditions. Additionally, we indicate where (and which) changes are in order for more general types of boundary conditions. Explicit examples of such generalizations are discussed in Section 6.3, which deals with the modifications of the estimates that arise in the applications in Sections 5.3 and 5.4.

6.1 Computation of the Y-bounds

Proposition 7. *The bounds*

$$Y_0 := \left|\Pi_0 A_N F_N\left(\hat{x}\right)\right|,$$
$$Y_{i,j} := \frac{t_i - t_{i-1}}{2\hat{\omega}} \sum_{k=N_i}^{N_g(N_i-1)+1} \left|\left[c^i_{k-1}(\hat{a}) - c^i_{k+1}(\hat{a})\right]_j\right| \frac{\nu_i^k}{k} + \left\|\Pi_{i,j} A_N F_N\left(\hat{x}\right)\right\|_{\nu_i},$$

where $1 \le i \le m$, $1 \le j \le n$, *satisfy* (3.7).

Proof. Let $1 \le i \le m$, $1 \le j \le n$ be arbitrary and note that

$$\left|\Pi_0\left(T\left(\hat{x}\right) - \hat{x}\right)\right| \le \left|\Pi_0 A\left(F\left(\hat{x}\right) - F_N\left(\hat{x}\right)\right)\right| + \left|\Pi_0 A F_N\left(\hat{x}\right)\right|, \tag{6.1}$$
$$\left\|\Pi_{i,j}\left(T\left(\hat{x}\right) - \hat{x}\right)\right\|_{\nu_i} \le \left\|\Pi_{i,j} A\left(F\left(\hat{x}\right) - F_N\left(\hat{x}\right)\right)\right\|_{\nu_i} + \left\|\Pi_{i,j} A F_N\left(\hat{x}\right)\right\|_{\nu_i}. \tag{6.2}$$

Next, observe that the only nonzero components of $F(\hat{x}) - F_N(\hat{x})$ are

$$\left(\Pi_{i,j}(F\left(\hat{x}\right) - F_N(\hat{x}))\right)_k = -\frac{(t_i - t_{i-1})}{4}\left[c^i_{k-1}(\hat{a}) - c^i_{k+1}(\hat{a})\right]_j, \qquad \text{for } N_i \le k \le N_g\left(N_i - 1\right) + 1.$$

Hence the result follows from (6.1) and (6.2). □

6.2 Computation of the Z-bounds

Let $x_1, x_2 \in B_r(0)$, $r > 0$ be arbitrary and recall the factorization in (3.6). We shall compute bounds $Z_{i,j}(r)$ and $Z_0(r)$ satisfying (3.8) and (3.10), respectively, by estimating the two terms in (3.6) separately. Throughout this section we write $x_1 = rv$ and $x_2 = rw$, where $v = \left(\omega_v, v^1, \ldots, v^m\right), w = \left(\omega_w, w^1, \ldots, w^m\right) \in B_1(0)$.

We start by computing a bound for $\left(I - A\widehat{A}\right)x_2$. To accomplish this we first state a result about the norm of linear operators C on $\mathcal{X}_\nu^N$, for which we introduce the notation

$$\Pi_0 C(\omega, 0) = C_0^0 \omega \qquad \Pi_0 C(0, a) = \sum_{\tilde{i}\tilde{j}\tilde{k}} (C_0^a)^{\tilde{i}\tilde{j}\tilde{k}} a_{\tilde{i}\tilde{j}\tilde{k}}$$
$$(\Pi_a C(\omega, 0))_{ijk} = (C_a^0)_{ijk}\,\omega \qquad (\Pi_a C(0, a))_{ijk} = \sum_{\tilde{i}\tilde{j}\tilde{k}} (C_a^a)^{\tilde{i}\tilde{j}\tilde{k}}_{ijk} a_{\tilde{i}\tilde{j}\tilde{k}}$$

where $i, \tilde{\imath} = 1, \ldots, m$ and $j, \tilde{\jmath} = 1, \ldots, n$ and $k, \tilde{k} = 0, \ldots, N_i - 1$ refer to the notation $a_{ijk} = ([a_k^i])_j$ for the Chebyshev coefficients introduced in Section 3.1.

Lemma 2. *Suppose* $C : \mathcal{X}_\nu^N \to \mathcal{X}_\nu^N$ *is a linear operator. Using the above notation, we define*

$$\eta_{ij} := \|(C_a^0)_{ij\cdot}\|_{\nu_i} \qquad \mu^{\tilde{i}\tilde{j}} := \|(C_0^a)^{\tilde{i}\tilde{j}\cdot}\|^*_{\nu_{\tilde{i}}}$$
$$\xi_{ij}^{\tilde{i}\tilde{j}\tilde{k}} := \|(C_a^a)^{\tilde{i}\tilde{j}\tilde{k}}_{ij\cdot}\|_{\nu_i} \qquad \xi_{ij}^{\tilde{i}\tilde{j}} := \|\xi_{ij}^{\tilde{i}\tilde{j}\cdot}\|^*_{\nu_{\tilde{i}}}.$$

Then

$$\|\Pi_0 C\|_{\mathscr{B}(\mathcal{X}_\nu^N, \mathbb{R})} \le |C_0^0| + \sum_{\tilde{\imath}=1}^m \sum_{\tilde{\jmath}=1}^n \mu^{\tilde{i}\tilde{j}},$$
$$\|\Pi_{i,j} C\|_{\mathscr{B}\left(\mathcal{X}_\nu^N, \ell^1_{\nu_i}\right)} \le \eta_{ij} + \sum_{\tilde{\imath}=1}^m \sum_{\tilde{\jmath}=1}^n \xi_{ij}^{\tilde{i}\tilde{j}}.$$

Proof. This follows from writing out the definitions of the norms. □

Remark 10. Explicit expressions for $\mu^{\tilde{i}\tilde{j}}$ and $\xi_{ij}^{\tilde{i}\tilde{j}}$ can be obtained by using Lemma 1.

We can now compute a bound for $\left(I - A\widehat{A}\right)x_2$:

Lemma 3. *Let $1 \leq i \leq m$, $1 \leq j \leq n$, and let h_0 and $h_{i,j} > 0$ denote the bounds*

$$\left\|\Pi_0 \left(I_N - A_N DF_N\left(\hat{x}\right)\right)\right\|_{\mathscr{B}\left(\mathcal{X}_\nu^N, \mathbb{R}\right)} \leq h_0, \qquad \left\|\Pi_{i,j} \left(I_N - A_N DF_N\left(\hat{x}\right)\right)\right\|_{\mathscr{B}\left(\mathcal{X}_\nu^N, \ell^1_{\nu_i}\right)} \leq h_{i,j},$$

provided by Lemma 2, where I_N is the identity on $\mathcal{X}_\nu^N$. Then

$$\left|\Pi_0 \left(I - A\widehat{A}\right) x_2\right| \leq h_0 r, \quad \left\|\Pi_{i,j} \left(I - A\widehat{A}\right) x_2\right\|_{\nu_i} \leq h_{i,j} r,$$

for all $1 \leq i \leq m$, $1 \leq j \leq n$.

Proof. It suffices to observe that

$$I - A\widehat{A} = \Pi_N \left(I - A\widehat{A}\right) = I_N - A_N DF_N\left(\hat{x}\right),$$

since the tails of A and $\widehat{A}$ are exact inverses of each other. □

The analysis of the second term in (3.6) is more complicated and requires one to analyze the infinite dimensional map F in more detail. Note that

$$\left(DF\left(\hat{x} + rv\right) - \widehat{A}\right) w = \left.\frac{\mathrm{d}}{\mathrm{d}\tau}\right|_{\tau=0} \left(F\left(\hat{x} + rv + \tau w\right) - F_N\left(\hat{x} + \tau w\right)\right) - \widehat{A}_\infty w, \tag{6.3}$$

where $\widehat{A}_\infty = \left(I - \Pi_N\right)\widehat{A}$, since $\Pi_N \widehat{A} = DF_N\left(\hat{x}\right)$. Furthermore, a straightforward computation shows that

$$\left(\left.\frac{\mathrm{d}}{\mathrm{d}\tau}\right|_{\tau=0} \Pi_i \left(F\left(\hat{x} + rv + \tau w\right) - F_N\left(\hat{x} + \tau w\right)\right)\right)_0 = 2\left(\sum_{k=N_i}^{\infty} \left(-1\right)^k w_k^i - \sum_{k=N_{i-1}}^{\infty} w_k^{i-1}\right), \tag{6.4}$$

for $1 < i \leq m$, and

$$\begin{aligned}\left(\left.\frac{\mathrm{d}}{\mathrm{d}\tau}\right|_{\tau=0} \Pi_i \left(F\left(\hat{x} + rv + \tau w\right) - F_N\left(\hat{x} + \tau w\right)\right)\right)_k = \quad & k\left(\omega_w v_k^i + \omega_v w_k^i\right) r \\ -\frac{t_i - t_{i-1}}{4} \left.\frac{\mathrm{d}}{\mathrm{d}\tau}\right|_{\tau=0} \Big(& c_{k-1}^i\left(\hat{a}^i + rv^i + \tau w^i\right) - c_{k-1}^i\left(\hat{a}^i + \tau \Pi_{N_i}\left(w^i\right)\right) \\ & - c_{k+1}^i\left(\hat{a}^i + rv^i + \tau w^i\right) + c_{k+1}^i\left(\hat{a}^i + \tau \Pi_{N_i}\left(w^i\right)\right)\Big),\end{aligned} \tag{6.5}$$

for $1 \leq i \leq m$, $1 \leq k \leq N_i - 1$, while

$$\begin{aligned}&\left(\left.\frac{\mathrm{d}}{\mathrm{d}\tau}\right|_{\tau=0} \Pi_i \left(F\left(\hat{x} + rv + \tau w\right) - F_N\left(\hat{x} + \tau w\right)\right) - \Pi_i \widehat{A}_\infty w\right)_k = \\ &k\left(\omega_w v_k^i + \omega_v w_k^i\right) r - \frac{t_i - t_{i-1}}{4} \left.\frac{\mathrm{d}}{\mathrm{d}\tau}\right|_{\tau=0} \left(c_{k-1}^i\left(\hat{a}^i + rv^i + \tau w^i\right) - c_{k+1}^i\left(\hat{a}^i + rv^i + \tau w^i\right)\right),\end{aligned} \tag{6.6}$$

for $1 \leq i \leq m$, $k \geq N_i$.

We start by computing a bound for (6.4):

Lemma 4. *Let $1 < i \leq m$, $1 \leq j \leq m$, then*

$$\left|\left(\left.\frac{\mathrm{d}}{\mathrm{d}\tau}\right|_{\tau=0} \Pi_{i,j} \left(F\left(\hat{x} + rv + \tau w\right) - F_N\left(\hat{x} + \tau w\right)\right)\right)_0\right| \leq \nu_i^{-N_i} + \nu_{i-1}^{-N_{i-1}}.$$

Proof. Define $\psi_i : \ell^1_{\nu_i} \to \mathbb{R}$ by $\psi_i(x) := 2\sum_{k=N_i}^{\infty} x_k$, and note that $\psi_i \in \left(\ell^1_{\nu_i}\right)^*$ for any $1 \leq i \leq m$, since $\nu_i > 1$. Furthermore, $\|\psi_i\|_{\nu_i} = \nu_i^{-N_i}$ by Lemma 1. Therefore, one can bound the components of (6.4) by $\nu_i^{-N_i} + \nu_{i-1}^{-N_{i-1}}$. □

Next, we compute component-wise bounds for the convolution terms in (6.5) for an arbitrary subdomain. Since the construction of these bounds is the same for each subdomain, we will fix and omit the superscript i whenever possible. Furthermore, to avoid additional clutter we shall denote the j-th component of a sequence a by a_j instead of $[a]_j$ whenever there is no chance of confusion.

Recall that the convolution terms are defined by

$$c(a) = \sum_{|\alpha| \leq N_g} g_\alpha a^\alpha,$$

where $a^\alpha = a_1^{\alpha_1} * \ldots * a_n^{\alpha_n}$, $a \in \ell^1_{(\nu_i,n)}$ and $N_g \in \mathbb{N}$ is the degree of the (polynomial) vector field. As mentioned before in the introduction, for the sake of simplicity, we shall restrict our attention to the case in which $N_g = 2$. In particular, note that

$$\sum_{|\alpha|=2} g_\alpha a^\alpha = \sum_{1 \leq l \leq s \leq n} g_{ls} a_l * a_s,$$

where $g_{ls} = g_{e_l + e_s}$ and $(e_j)_{j=1}^n$ are the unit vectors in $\mathbb{R}^n$.

A straightforward computation shows that

$$\begin{aligned} &\frac{\mathrm{d}}{\mathrm{d}\tau}\bigg|_{\tau=0} \left(c\left(\hat{a} + rv + \tau w\right) - c\left(\hat{a} + \tau \Pi_{N_i}(w)\right)\right) \\ &= \sum_{j=1}^{n} g_{e_j} [\tilde{w}]_j + \sum_{1 \leq l \leq s \leq n} g_{ls} \left(\tilde{w}_l * \hat{a}_s + \tilde{w}_s * \hat{a}_l + r\left(w_l * v_s + w_s * v_l\right)\right), \end{aligned} \tag{6.7}$$

where

$$\tilde{w} = \begin{cases} \mathbf{0}_n, & 0 \leq k \leq N_i - 1, \\ w_k, & k \geq N_i. \end{cases}$$

The following lemma is key in computing bounds for the linear terms in (6.7):

Lemma 5. *Let $a \in \ell^1_{\nu_i}$ be such that $a_k = 0$ for $k \geq N_i$. Define $\Psi_{a,k} : \ell^1_{\nu_i} \to \mathbb{R}$ by*

$$\Psi_{a,k}(x) := (\tilde{x} * a)_{k-1} - (\tilde{x} * a)_{k+1}, \qquad \text{for } 1 \leq k \leq N_i - 1,$$

where $\tilde{x}$ is defined by

$$\tilde{x} = \begin{cases} 0, & 0 \leq k \leq N_i - 1, \\ x_k, & k \geq N_i. \end{cases}$$

Then $\Psi_{a,k} \in \left(\ell^1_{\nu_i}\right)^*$ for $1 \leq k \leq N_i - 1$, and

$$\|\Psi_{a,k}\|^*_{\nu_i} = \frac{1}{2} \max\left(\left\{\nu_i^{-l} \left|a_{|k-1-l|} - a_{|k+1-l|}\right|\right\}_{l=N_i}^{l=k+N_i-2}, \nu_i^{-(k+N_i-1)} \left|a_{|N_i-2|}\right|, \nu_i^{-(k+N_i)} \left|a_{N_i-1}\right|\right).$$

Proof. Let $x \in \ell^1_{\nu_i}$, $k \in \mathbb{N}_0$ be arbitrary and observe that

$$(\tilde{x} * a)_k = \sum_{k_1=N_i}^{k+N_i-1} x_{k_1} a_{|k-k_1|}, \tag{6.8}$$

since $\tilde{x}_{k_1} = 0$, $a_{k_2} = 0$, for $0 \leq k_1 \leq N_i - 1$ and $k_2 \geq N_i$, respectively. Next, note that $\Psi_{a,k} \in \left(\ell^1_{\nu_i}\right)^*$ by Proposition 3, and

$$\Psi_{a,k}(\varepsilon_l) = \begin{cases} \frac{\nu_i^{-l}}{2}\left(a_{|k-1-l|} - a_{|k+1-l|}\right), & N_i \leq l \leq k + N_i - 2, \\ -\frac{\nu_i^{-l}}{2} a_{|k+1-l|}, & l = k + N_i - 1, k + N_i \\ 0, & \text{otherwise.} \end{cases}$$

Now use Lemma 1 to obtain the stated formula for $\|\Psi_{a,k}\|^*_{\nu_i}$. □

Corollary 2. *Let $1 \le i \le m$ and $1 \le k \le N_i - 1$, then*

$$\left| \left(\sum_{j=1}^{n} g_{e_j} \left[\tilde{w}\right]_j + \sum_{1 \le l \le s \le n} g_{ls} \left(\tilde{w}_l * \hat{a}_s + \tilde{w}_s * \hat{a}_l \right) \right)_{k-1} - \left(\sum_{j=1}^{n} g_{e_j} \left[\tilde{w}\right]_j + \sum_{1 \le l \le s \le n} g_{ls} \left(\tilde{w}_l * \hat{a}_s + \tilde{w}_s * \hat{a}_l \right) \right)_{k+1} \right|$$

is bounded by (using the Kronecker δ)

$$B_k^i := \delta_{k,N_i-1} \frac{1}{2} \nu_i^{-N_i} \sum_{j=1}^{n} \left| g_{e_j} \right| + \sum_{1 \le l \le s \le n} |g_{ls}| \left(\left\| \Psi_{\hat{a}_l^i,k} \right\|_{\nu_i}^* + \left\| \Psi_{\hat{a}_s^i,k} \right\|_{\nu_i}^* \right). \tag{6.9}$$

We are now ready to construct bounds for

$$\left\| \Pi_{i,j} \Pi_N A \left(DF\left(\hat{x} + x_1\right) - \widehat{A} \right) x_2 \right\|_{\nu_i}. \tag{6.10}$$

There are two boundary conditions that we need to deal with separately, namely the phase condition and the periodicity condition (the "internal" boundary conditions between successive domains will be dealt with uniformly). We deal with these two bounds in such a way that the method can be easily adapted to deal with other boundary conditions. Hence, for the moment, assume that there exist bounds $\Lambda_{0,1},\ \Lambda_{0,2} > 0$, and $\Lambda_{1,1},\ \Lambda_{1,2} \in \mathbb{R}^n_{\ge 0}$, such that

$$\left| \frac{\mathrm{d}}{\mathrm{d}\tau} \right|_{\tau=0} \Pi_0 \left(F\left(\hat{x} + rv + \tau w\right) - F_N\left(\hat{x} + \tau w\right) \right) \Big| \le \Lambda_{0,1} + r\Lambda_{0,2}, \tag{6.11}$$

$$\left| \frac{\mathrm{d}}{\mathrm{d}\tau} \right|_{\tau=0} \left(\Pi_1 \left(F\left(\hat{x} + rv + \tau w\right) - F_N\left(\hat{x} + \tau w\right) \right) \right)_0 \Big| \le \Lambda_{1,1} + r\Lambda_{1,2}, \tag{6.12}$$

for any $v, w \in B_1(0)$. Explicit expressions for these bounds are given explicitly in Remark 11 for periodic boundary conditions.

We define $\tilde{Z}_1 \in \mathbb{R}^{1+n\sum_{i=1}^m N_i}$ by

$$\Pi_0 \tilde{Z}_1 := \Lambda_{0,1}, \qquad \Pi_{N_1} \tilde{Z}_1 := \begin{bmatrix} \Lambda_{1,1} \\ \frac{t_1 - t_0}{4} \left[B_k^1\right]_{k=1}^{N_1-1} \end{bmatrix}, \qquad \Pi_{N_i} \tilde{Z}_1 := \begin{bmatrix} \left(\nu_i^{-N_i} + \nu_{i-1}^{-N_{i-1}} \right) \cdot \mathbf{1}_n \\ \frac{t_i - t_{i-1}}{4} \left[B_k^i\right]_{k=1}^{N_i-1} \end{bmatrix},$$

with B_k^i defined in (6.9), and we set $Z_1 = |A_N| \, \tilde{Z}_1$.

Proposition 8. *Let $1 \le i \le m$, $1 \le j \le n$, then*

$$\left| \Pi_0 A \left(DF\left(\hat{x} + x_1\right) - \widehat{A} \right) x_2 \right| \le \Pi_0 Z_1 r + \gamma \left\| \Pi_0 A_N \right\|_{\mathcal{B}(\mathcal{X}_\nu^N, \mathbb{R})} r^2,$$

$$\left\| \Pi_{i,j} \Pi_N A \left(DF\left(\hat{x} + x_1\right) - \widehat{A} \right) x_2 \right\|_{\nu_i} \le \left\| \Pi_{i,j} Z_1 \right\|_{\nu_i} r + \gamma \left\| \Pi_{i,j} A_N \right\|_{\mathcal{B}\left(\mathcal{X}_\nu^N, \ell^1_{\nu_i}\right)} r^2,$$

where the operator norms can be evaluated using Lemma 2, and

$$\gamma := \max \left(\{\Lambda_{0,2}\} \cup \left\{ \left| \Lambda_{1,2} + 2\left(N_1 - 1\right) + \frac{\left(t_1 - t_0\right)\left(2\nu_1^2 + 1\right)}{2\nu_1} \sum_{|\alpha|=2} |g_\alpha| \right|_\infty \right\} \cup \left\{ \left| 2\left(N_i - 1\right) + \frac{\left(t_i - t_{i-1}\right)\left(2\nu_i^2 + 1\right)}{2\nu_i} \sum_{|\alpha|=2} |g_\alpha| \right|_\infty : 2 \le i \le m \right\} \right).$$

Proof. First observe that

$$\left| \Pi_0 \left(DF\left(\hat{x} + x_1\right) - \widehat{A} \right) x_2 \right| \le \Lambda_{0,1} r + \Lambda_{0,2} r^2$$

by (6.11) and

$$\left|\Pi_{N_1}\left(DF\left(\hat{x}+x_1\right)-\widehat{A}\right)x_2\right| \leq \Pi_{N_1}\left(\tilde{Z}_1\right)r+\tilde{Z}_{2,1}r^2, \tag{6.13}$$

where

$$(\tilde{Z}_{2,1})_k := \begin{cases} \Lambda_{1,2}, & k=0, \\ k\left(|v_k|+|w_k|\right)+\dfrac{t_1-t_0}{4}\displaystyle\sum_{1\leq l\leq s\leq n}|g_{ls}|\left(\left|(w_l*v_s)_{k-1}\right|\right. & \\ \qquad \left.+\left|(w_s*v_l)_{k-1}\right|+\left|(w_l*v_s)_{k+1}\right|+\left|(w_s*v_l)_{k+1}\right|\right), & 1\leq k\leq N_1-1, \end{cases}$$

by (6.12) and Corollary 2. Furthermore, the quadratic part of (6.13) is estimated by

$$\|[\tilde{Z}_{2,1}]\|_{(\nu_1,n)} \leq \max_{1\leq j\leq n}\left([\Lambda_{1,2}]_j+2\left(N_1-1\right)+\frac{\left(t_1-t_0\right)\left(2\nu_1^2+1\right)}{2\nu_1}\sum_{|\alpha|=2}\left|[g_\alpha]_j\right|\right).$$

Similarly,

$$\left|\Pi_{N_i}\left(DF\left(\hat{x}+x_1\right)-\widehat{A}\right)x_2\right| \leq \Pi_{N_i}\left(\tilde{Z}_1\right)r+\tilde{Z}_{2,i}r^2,$$

where

$$(\tilde{Z}_{2,i})_k = \begin{cases} \mathbf{0}_n, & k=0, \\ k\left(|v_k|+|w_k|\right)+\dfrac{t_i-t_{i-1}}{4}\displaystyle\sum_{1\leq l\leq s\leq n}|g_{ls}|\left(\left|(w_l*v_s)_{k-1}\right|\right. & \\ \qquad \left.+\left|(w_s*v_l)_{k-1}\right|+\left|(w_l*v_s)_{k+1}\right|+\left|(w_s*v_l)_{k+1}\right|\right), & 1\leq k\leq N_i-1, \end{cases}$$

and the quadratic part is estimated by

$$\|[\tilde{Z}_{2,i}]\|_{(\nu_i,n)} \leq \max_{1\leq j\leq n}\left(2\left(N_i-1\right)+\frac{\left(t_i-t_{i-1}\right)\left(2\nu_i^2+1\right)}{2\nu_i}\sum_{|\alpha|=2}\left|[g_\alpha]_j\right|\right).$$

Combining these estimates, we can now bound $A\left(DF\left(\hat{x}+x_1\right)-\widehat{A}\right)x_2$ as asserted. □

Remark 11. In the current setting for periodic orbits we have that

$$\begin{aligned} &\frac{\mathrm{d}}{\mathrm{d}\tau}\bigg|_{\tau=0}\Pi_0\left(F\left(\hat{x}+rv+\tau w\right)-F_N\left(\hat{x}+\tau w\right)\right)=0, \\ &\left(\frac{\mathrm{d}}{\mathrm{d}\tau}\bigg|_{\tau=0}\Pi_1\left(F\left(\hat{x}+rv+\tau w\right)-F_N\left(\hat{x}+\tau w\right)\right)\right)_0 = 2\left(\sum_{k=N_1}^{\infty}\left(-1\right)^k w_k^1-\sum_{k=N_m}^{\infty}w_k^m\right). \end{aligned}$$

Therefore, by the same computation as in Lemma 4, it suffices to set

$$\Lambda_{1,1}=\left(\nu_1^{-N_1}+\nu_m^{-N_m}\right)\cdot\mathbf{1}_n, \quad \Lambda_{1,2}=\mathbf{0}_n, \quad \Lambda_{0,1}=\Lambda_{0,2}=0.$$

It remains to bound the $\ell^1_{\nu_i}$-norm of (6.6) for $k\geq N_i$. Observe that

$$\frac{\mathrm{d}}{\mathrm{d}\tau}\bigg|_{\tau=0}c\left(\hat{a}+rv+\tau w\right)=\sum_{j=1}^{n}g_j\left[w\right]_j+\sum_{1\leq l\leq s\leq n}g_{ls}\left(w_l*\hat{a}_s+w_s*\hat{a}_l+r\left(w_l*v_s+w_s*v_l\right)\right). \tag{6.14}$$

Lemma 6. *Let $a \in \ell^1_{\nu_i}$ be such that $a_k = 0$ for $k \geq N_i$. Define $\varphi_a^-, \varphi_a^+ : \ell^1_{\nu_i} \to \mathbb{R}$ by*

$$\varphi_a^-(x) := \sum_{k=N_i-1}^{\infty} (x * |a|)_k \frac{\nu_i^k}{k+1}, \quad \varphi_a^+(x) := \sum_{k=N_i+1}^{\infty} (x * |a|)_k \frac{\nu_i^k}{k-1}.$$

Then $\varphi_a^-, \varphi_a^+ \in \left(\ell^1_{\nu_i}\right)^*$, and $\|\varphi_a^-\|^*_{\nu_i} = \frac{1}{2}\Gamma_a^-$, $\|\varphi_a^+\|^*_{\nu_i} = \frac{1}{2}\Gamma_a^+$, where

$$\Gamma_a^- := \max\left(\left\{2\left|a_{N_i-1}\right| \frac{\nu_i^{N_i-1}}{N_i}\right\} \cup \left\{\sum_{k=N_i-1-l}^{N_i-1} \left|a_{|k|}\right| \frac{\nu_i^k}{k+l+1} : 1 \leq l \leq 2(N_i-1)\right\}\right),$$

$$\Gamma_a^+ := \max\left\{\sum_{k=N_i+1-l}^{N_i-1} \left|a_{|k|}\right| \frac{\nu_i^k}{k+l-1} : 2 \leq l \leq 2N_i\right\}.$$

Proof. It follows directly from Proposition 3 that $\varphi_a^-, \varphi_a^+ \in \left(\ell^1_{\nu_i}\right)^*$. Next, we consider the computation of $\|\varphi_a^-\|_{\nu_i}$ (the computation of $\|\varphi_a^+\|_{\nu_i}$ is similar). Let $k \geq N_i - 1$ be arbitrary and observe that

$$(x * |a|)_k = \sum_{k_1=k-N_i+1}^{k+N_i-1} x_{k_1} \left|a_{|k-k_1|}\right|,$$

since $a_{k_2} = 0$ for $k_2 \geq N_i$. Therefore,

$$\varphi_a^-(\varepsilon_l) = \begin{cases} \left|a_{N_i-1}\right| \frac{\nu_i^{N_i-1}}{N_i}, & l = 0, \\ \frac{1}{2} \sum_{k=N_i-1-l}^{N_i-1} \left|a_{|k|}\right| \frac{\nu_i^k}{k+l+1}, & 1 \leq l \leq 2(N_i-1), \\ \frac{1}{2} \sum_{k=1-N_i}^{N_i-1} \left|a_{|k|}\right| \frac{\nu_i^k}{k+l+1}, & l \geq 2(N_i-1). \end{cases}$$

In particular, note that $\varphi_a^-(\varepsilon_l)$ is decreasing for $l \geq 2(N_i-1)$. Hence

$$\left\|\varphi_a^-\right\|^*_{\nu_i} = \sup_{l \in \mathbb{N}_0} \left|\varphi_a^-(\varepsilon_l)\right| = \frac{1}{2}\Gamma_a^-$$

by Lemma 1.

An analogous computation yields $\|\varphi_a^+\|^*_{\nu_i} = \frac{1}{2}\Gamma_a^+$. □

Corollary 3 (Estimates for the tail)**.** *Define*

$$d_1^i := \frac{\nu_i^2+1}{\nu_i N_i} \sum_{j=1}^{n} \left|g_{e_j}\right| + \sum_{1 \leq l \leq s \leq n} |g_{ls}| \left(\nu_i \left(\Gamma^-_{\hat{a}_l^i} + \Gamma^-_{\hat{a}_s^i}\right) + \frac{1}{\nu_i}\left(\Gamma^+_{\hat{a}_l^i} + \Gamma^+_{\hat{a}_s^i}\right)\right),$$

$$d_2^i := \frac{2\left(\nu_i^2+1\right)}{\nu_i N_i} \sum_{|\alpha|=2} |g_\alpha|,$$

then

$$2\sum_{k=N_i}^{\infty} \left|\frac{\mathrm{d}}{\mathrm{d}\tau}\right|_{\tau=0} \left(c_{k-1}\left(\hat{a}^i + rv + \tau w\right) - c_{k+1}\left(\hat{a}^i + rv + \tau w\right)\right) \left| \frac{\nu_i^k}{k} \leq d_1^i + r d_2^i.\right.$$

Proof. First note that

$$2\sum_{k=N_i}^{\infty} \left|\frac{\mathrm{d}}{\mathrm{d}\tau}\right|_{\tau=0} c_{k-1}\left(\hat{a}^i + rv + \tau w\right) \left| \frac{\nu_i^k}{k} = 2\nu_i \sum_{k=N_i-1}^{\infty} \left|\frac{\mathrm{d}}{\mathrm{d}\tau}\right|_{\tau=0} c_k\left(\hat{a}^i + rv + \tau w\right) \right| \frac{\nu_i^k}{k+1}.$$

Next, observe that

$$2\sum_{k=N_i-1}^{\infty}\left|\sum_{j=1}^{n}g_{e_j}\left[w_k\right]_j\right|\frac{\nu_i^k}{k+1}\leq\frac{1}{N_i}\sum_{j=1}^{n}\left|g_{e_j}\right|\left\|\left[w\right]_j\right\|_{\nu_i}\leq\frac{1}{N_i}\sum_{j=1}^{n}\left|g_{e_j}\right|,$$

while

$$2\sum_{k=N_i-1}^{\infty}\left|\left(w_l*\hat{a}_s^i\right)_k\right|\frac{\nu_i^k}{k+1}\leq 2\varphi^-_{\hat{a}_s^i}\left(|w_l|\right)\leq\Gamma^-_{\hat{a}_s^i},$$

and

$$2\sum_{k=N_i-1}^{\infty}\left|\left(w_l*rv_s\right)_k\right|\frac{\nu_i^k}{k+1}\leq\frac{r}{N_i}\left\|w_l*v_s\right\|_{\nu_i}\leq\frac{r}{N_i},$$

for any $l,s\in\{1,\dots,n\}$ by Proposition 3, Lemma 6, and since $v,w\in B_1(0)$. Therefore,

$$2\sum_{k=N_i}^{\infty}\left|\frac{\mathrm{d}}{\mathrm{d}\tau}\right|_{\tau=0}c_{k-1}\left(\hat{a}^i+rv+\tau w\right)\left|\frac{\nu_i^k}{k}\leq\nu_i\left(\frac{1}{N_i}\sum_{j=1}^{n}\left|g_{e_j}\right|+\sum_{1\leq l\leq s\leq n}\left|g_{ls}\right|\left(\Gamma^-_{\hat{a}_l^i}+\Gamma^-_{\hat{a}_s^i}+\frac{2r}{N_i}\right)\right),\right.$$

by (6.14). An analogous computation shows that

$$2\sum_{k=N_i}^{\infty}\left|\frac{\mathrm{d}}{\mathrm{d}\tau}\right|_{\tau=0}c_{k+1}\left(\hat{a}^i+rv+\tau w\right)\left|\frac{\nu_i^k}{k}\leq\frac{1}{\nu_i}\left(\frac{1}{N_i}\sum_{j=1}^{n}\left|g_{e_j}\right|+\sum_{1\leq l\leq s\leq n}\left|g_{ls}\right|\left(\Gamma^+_{\hat{a}_l^i}+\Gamma^+_{\hat{a}_s^i}+\frac{2r}{N_i}\right)\right),\right.$$

which completes the proof of the lemma. □

We are now ready to define the Z-bounds:

Proposition 9. *The bounds*

$$\begin{aligned}Z_{i,j}\left(r\right):&=\left[\gamma\left\|\Pi_{i,j}A_N\right\|_{\mathcal{B}\left(\mathcal{X}_\nu^N,\ell^1_{\nu_i}\right)}+\frac{1}{\hat{\omega}}\left(\frac{t_i-t_{i-1}}{4}\left[d_2^i\right]_j+2\right)\right]r^2\\&\quad+\left[h_{i,j}+\left\|\Pi_{i,j}\left(Z_1\right)\right\|_{\nu_i}+\frac{t_i-t_{i-1}}{4\hat{\omega}}\left[d_1^i\right]_j\right]r,\\Z_0\left(r\right):&=\gamma\left\|\Pi_0A_N\right\|_{\mathcal{B}\left(\mathcal{X}_\nu^N,\mathbb{R}\right)}r^2+\left(h_0+\Pi_0\left(Z_1\right)\right)r,\end{aligned}$$

where $1\leq i\leq m$, $1\leq j\leq n$, satisfy (3.8) and (3.10), respectively.

Proof. First observe that

$$\begin{aligned}&\left(\Pi_iA\left(DF\left(\hat{x}+w_1\right)-\widehat{A}\right)w\right)_k=\\&\frac{\omega_wv_k^i+\omega_vw_k^i}{\hat{\omega}}r-\frac{t_i-t_{i-1}}{4\hat{\omega}k}\frac{\mathrm{d}}{\mathrm{d}\tau}\bigg|_{\tau=0}\left(c_{k-1}\left(\hat{a}+rv+\tau w\right)-c_{k+1}\left(\hat{a}+rv+\tau w\right)\right)\end{aligned}$$

for all $k\geq N_i$ by (6.3) and (6.6), and

$$\sum_{k=N_i}^{\infty}\left|\omega_wv_k^i+\omega_vw_k^i\right|\nu_i^k\leq\mathbf{1}_n,\tag{6.15}$$

since $v,w\in B_1(0)$. Now recall the decomposition in (3.6) and combine (6.15), Lemma 3, Proposition 8, and Corollary 3 to obtain the result. □

6.3 Modifications for non-periodic boundary conditions

In Section 5.3 an equation representing arc-length continuation is added to the system, accompanied by an extra a priori unknown parameter. In Section 5.4 the periodic boundary conditions are replaced by boundary conditions that guarantee that the solution ends up in the local stable and unstable manifolds. The adaptations of the estimates to these modified problems are presented in Sections 6.3.1 and 6.3.2, respectively.

6.3.1 Periodic solutions near the homoclinic orbit

In this section we incorporate the necessary adjustments for the modified problem introduced in section 5.3. First, observe that we will have an additional radii-polynomial p_{-1} which corresponds to the equation for ρ. In particular, the additional bound Y_{-1} is given by

$$Y_{-1} := \left|\Pi_{-1} A_N F_N\left(\hat{x}\right)\right|,$$

and the formulae for the other Y-bounds remain the same.

Recall that the Z-bounds were derived by estimating the two terms in (3.6). In particular, one can derive bounds for the norm of linear operators on $\mathcal{X}_\nu^N$ in exactly the same way as before as in Lemma 2, and then use Lemma 3 to compute a bound for $\left(I - A\widehat{A}\right) x_2$. The changes in the bounds for the second term, $A\left(DF\left(\hat{x}+x_1\right) - \widehat{A}\right) x_2$, are more subtle, since ρ is now to be interpreted as an unknown variable as well.

To identify the differences, denote the approximate solution by $\hat{x} = \left(\hat{\rho}, \hat{\omega}, \hat{a}^1, \ldots, \hat{a}^m\right)$, write $x_1 = rv$, $x_2 = rw$, where $v = \left(\rho_1, \omega_1, v^1, \ldots, v^m\right), w = \left(\rho_2, \omega_2, w^1, \ldots, w^m\right) \in B_1(0)$, and recall that the bounds for $A\left(DF\left(\hat{x}+x_1\right) - \widehat{A}\right) x_2$ were obtained by computing estimates for (6.5) and (6.6). Furthermore, observe that the additional equation for ρ has no contribution to this part of the analysis, since the equation is linear and therefore

$$\frac{\mathrm{d}}{\mathrm{d}\tau}\bigg|_{\tau=0} \Pi_{-1}\left(F\left(\hat{x} + rv + \tau w\right) - F_N\left(\hat{x} + \tau w\right)\right) = 0.$$

Next, note that the convolution terms c^i are the only functions in the definition of F which depend on ρ, since g_{e_1} is the only coefficient in the Lorenz-system which depends on ρ. Consequently, a straightforward computation shows that the term

$$\begin{bmatrix} 0 \\ r\left(\rho_1 \left[w^i\right]_1 + \rho_2 \left[v^i\right]_1\right) \\ 0 \end{bmatrix},$$

needs to be added to the right-hand side of (6.7), and $g_{e_1}\left[\tilde{w}^i\right]_1 = g_{e_1}\left(\hat{\rho}\right)\left[\tilde{w}^i\right]_1$. To incorporate this extra term in the estimates for (6.10) one needs to modify Proposition 8 by setting

$$\gamma := \max\left\{\left|2\left(N_i - 1\right) + \frac{\left(t_i - t_{i-1}\right)\left(2\nu_i^2 + 1\right)}{2\nu_i}\left(\sum_{|\alpha|=2}\left|g_\alpha\right| + \begin{bmatrix} 0 \\ 1 \\ 0 \end{bmatrix}\right)\right|_\infty : 1 \le i \le m\right\}.$$

Similarly, terms

$$\begin{pmatrix} 0 \\ \rho_2\left[\hat{a}^i\right]_1 \\ 0 \end{pmatrix} + \begin{pmatrix} 0 \\ \rho_2\left[v^i\right]_1 + \rho_1\left[w^i\right]_1 \\ 0 \end{pmatrix} r.$$

need to be added to the right-hand side of (6.14).

Therefore, by analogous computations as in the proof of Corollary 3, the tail-estimates in Corollary 3 remain valid if we add the terms

$$\frac{2\nu_i^{N_i}\left|\left[\hat{a}^i_{N_i-1}\right]_1\right|}{N_i} \qquad \text{and} \qquad \frac{2\left(\nu_i^2+1\right)}{N_i\nu_i},$$

to the expressions for $\left[d_1^i\right]_2$ and $\left[d_2^i\right]_2$, respectively.

The above modifications account for all the necessary changes in the estimates, and the extra formula for the additional bound Z_{-1} is given by

$$Z_{-1}(r) := \gamma \left\| \Pi_{-1} A_N \right\|_{\mathcal{B}(\mathcal{X}_\nu^N, \mathbb{R})} r^2 + \left(h_{-1} + \Pi_{-1} \left(Z_1 \right) \right) r.$$

6.3.2 Heteroclinic orbit

In this section we identify the differences in the construction of the bounds for the connecting orbit discussed in section 5.4. We start by identifying the differences in the Y-bounds. We write $\hat{x} = \left(\hat{\phi}, \hat{\alpha}, \hat{a}^1, \ldots, \hat{a}^m\right)$ and observe that the main difference in the computation of the Y-bounds, as performed in Proposition 7, is caused by the following two terms being nonzero:

$$\left[\Pi_{0,j} \left(F\left(\hat{x}\right) - F_N\left(\hat{x}\right) \right) \right]_{j=1}^3 = \left(Q - Q_{N_s} \right) \circ \Theta_\mu(\hat{\phi}),$$

and

$$\left(\Pi_1 \left(F\left(\hat{x}\right) - F_N\left(\hat{x}\right) \right) \right)_0 = \left(P - P_{N_u} \right) \left(\hat{\alpha} \right).$$

Consequently, we have additional bounds corresponding to the finite dimensional part of $A(F\left(\hat{x}\right) - F_N\left(\hat{x}\right))$, which previously had no contribution at all.

The required modifications are as follows: set

$$\delta := \left| A_N \right| \begin{pmatrix} \delta_s \cdot \mathbf{1}_n \\ \delta_u \cdot \mathbf{1}_n \\ \mathbf{0}_{n\left(-1+\sum_{i=1}^m N_i\right)} \end{pmatrix},$$

add the bounds $\left\| \Pi_{i,j} \left(\delta \right) \right\|_{\nu_i}$ to $Y_{i,j}$ in Proposition 7, define (instead of Y_0) the bounds

$$Y_{0,j} := \left| \Pi_{0,j} A_N F_N\left(\hat{x}\right) \right| + \Pi_{0,j} \left(\delta \right),$$

where $1 \leq j \leq n$, and change the factor $\dfrac{1}{\hat{\omega}}$ into L.

Next, we consider the computation of the Z-bounds by considering the decomposition in (3.6) again. As before, the main differences occur in the bounds for $A\left(DF\left(\hat{x} + x_1\right) - \widehat{A}\right) x_2$, which stem from the fact that there is no dependence on ω anymore, whereas dependencies on ϕ and α need to be incorporated. To identify the differences, write $x_1 = rv$ and $x_2 = rw$, where $v = \left(\phi_1, \alpha_1, v^1, \ldots, v^m\right)$, $w = \left(\phi_2, \alpha_2, w^1, \ldots, w^m\right) \in B_1(0)$.

The main differences in the right-hand sides of (6.5) and (6.6) in the current setting are that the term $k\left(\omega_2 v_k^i + \omega_1 w_k^i\right) r$ is not present, and the factors $\frac{t_i - t_{i-1}}{4}$ need to be multiplied by L. To incorporate these changes into the bounds for (6.10) we only need to modify Proposition 8 by setting

$$\gamma := \max \left(\left\{ \left| \Lambda_{0,2} \right|_\infty \right\} \cup \left\{ \left| \Lambda_{1,2} + \frac{L\left(t_1 - t_0\right)\left(2\nu_1^2 + 1\right)}{2\nu_1} \sum_{|\alpha|=2} \left| g_\alpha \right| \right|_\infty \right\} \cup \right.$$
$$\left. \left\{ \left| \frac{L\left(t_i - t_{i-1}\right)\left(2\nu_i^2 + 1\right)}{2\nu_i} \sum_{|\alpha|=2} \left| g_\alpha \right| \right|_\infty : 2 \leq i \leq m \right\} \right).$$

Here the extra bounds $\Lambda_{0,1}$, $\Lambda_{0,2} \in \mathbb{R}_+^3$ and $\Lambda_{1,1}$, $\Lambda_{1,2} \in \mathbb{R}_+^3$, defined analogously as in (6.11) and (6.12), respectively, can be obtained by computing estimates for

$$\left. \frac{\mathrm{d}}{\mathrm{d}\tau} \right|_{\tau=0} \Pi_{0,j} \left(F\left(\hat{x} + rv + \tau w\right) - F_N\left(\hat{x} + \tau w\right) \right) = 2 \sum_{k=N_m}^{\infty} \left[w_k^m \right]_j$$
$$- \left. \frac{\mathrm{d}}{\mathrm{d}\tau} \right|_{\tau=0} \left(Q_{N_s} \circ \Theta_\mu \left(\hat{\phi} + r\phi_1 + \tau\phi_2 \right) - Q_{N_s} \circ \Theta_\mu \left(\hat{\phi} + \tau\phi_2 \right) + h_s \circ \Theta_\mu \left(\hat{\phi} + r\phi_1 + \tau\phi_2 \right) \right)$$

for $1 \leq j \leq 3$, and

$$\left.\frac{\mathrm{d}}{\mathrm{d}\tau}\right|_{\tau=0} \left(\Pi_1\big(F\left(\hat{x}+rv+\tau w\right)-F_N\left(\hat{x}+\tau w\right)\big)\right)_0 = 2\sum_{k=N_1}^{\infty}\left(-1\right)^k w_k^1$$
$$-\left.\frac{\mathrm{d}}{\mathrm{d}\tau}\right|_{\tau=0} \big(P_{N_u}\left(\hat{\alpha}+r\alpha_1+\tau\alpha_2\right)-P_{N_u}\left(\hat{\alpha}+\tau\alpha_2\right)+h_u\left(\hat{\alpha}+r\alpha_1+\tau\alpha_2\right)\big),$$

respectively, where $h_u = P - P_{N_u}$ and $h_s = Q - Q_{N_s}$. The series involving w^m and w^1 in the latter two expressions can be bounded in the same way as in Lemma 4. The terms associated to the parameterizations P and Q can be bounded by using a combination of analysis and interval arithmetic. In particular, this involves the choice of an a priori radius $r^* > 0$ in order to compute uniform bounds for $|DP_{N_u}\left(\alpha^* + r\alpha_1\right)|$ and $|D\left(Q_{N_s}\circ\Theta_\mu\right)\left(\phi^* + r\phi_1\right)|$ for $0 < r < r^*$, where $|\phi_1|$, $|\alpha_1|_2 \leq 1$. The reader is referred to [22] for the details.

The final changes to be made are in Proposition 9: the Z-bounds are now defined by

$$\begin{aligned} Z_{i,j}\left(r\right) :&= \left[\gamma\left\|\Pi_{i,j}A_N\right\|_{\mathcal{B}\left(\mathcal{X}_\nu^N,\ell^1_{\nu_i}\right)} + \frac{L\left(t_i-t_{i-1}\right)}{4}\left[d_2^i\right]_j\right]r^2 \\ &\quad + \left[h_{i,j} + \left\|\Pi_{i,j}\left(Z_1\right)\right\|_{\nu_i} + \frac{L\left(t_i-t_{i-1}\right)}{4}\left[d_1^i\right]_j\right]r, \\ Z_{0,j}\left(r\right) :&= \gamma\left\|\Pi_{0,j}A_N\right\|_{\mathcal{B}\left(\mathcal{X}_\nu^N,\mathbb{R}\right)}r^2 + \left(h_{0,j} + \Pi_{0,j}\left(Z_1\right)\right)r, \end{aligned}$$

where $1 \leq i \leq m$ and $1 \leq j \leq 3$.

References

[1] *CAPD: Computer assisted proofs in dynamics, a package for rigorous numerics.* `http://capd.ii.uj.edu.pl`.

[2] *COSY.* `http://bt.pa.msu.edu/index.htm`.

[3] G. Arioli and H. Koch, *Computer-Assisted Methods for the Study of Stationary Solutions in Dissipative Systems, Applied to the Kuramoto-Sivashinski Equation*, Archive for Rational Mechanics and Analysis **197** (2010), no. 3, 1033–1051.

[4] ———, *Existence and stability of traveling pulse solutions of the FitzHugh-Nagumo equation*, Nonlinear Analysis: Theory, Methods and Applications **113** (2015), 51–70.

[5] A.W. Baker, M. Dellnitz, and O. Junge, *A topological method for rigorously computing periodic orbits using fourier modes*, Discrete and Continuous dynamical systems **13** (2005), no. 4, 901–920.

[6] R. Barrio, A. Dena, and W. Tucker, *A database of rigorous and high-precision periodic orbits of the Lorenz model*, Computer Physics Communications **194** (2015), 76–83.

[7] M. Berz and K. Makino, *Verified integration of ODEs and Flows Using Differential Algebraic Methods on High-Order Taylor Models*, Reliable computing **4** (1997), 361–369.

[8] J.P. Boyd, *Chebyshev and Fourier Spectral Methods*, Dover Publishers, 2001.

[9] M. Breden, J.P. Lessard, and M. Vanicat, *Global bifurcation diagram of steady states of systems of PDEs via rigorous numerics: a 3-component reaction-diffusion system*, Acta Applicandae Mathematicae **128** (2013), no. 1, 113–152.

[10] B. Breuer, J. Horák, P.J. McKenna, and M. Plum, *A computer-assisted existence and multiplicity proof*, J. Differential Equations **224** (2005), no. 1, 60–97.

[11] X. Cabré, E. Fontich, and R. de la Llave, *The parameterization method for invariant manifolds III: overview and applications*, J.Differential Equations **218** (2005), no. 2, 444–515.

[12] B. Coomes, H. Koçak, and K. Palmer, *Transversal connecting orbits from shadowing*, Numerische Mathematik **106** (2007), no. 3, 427–469.

[13] S. Day, Y. Hiraoka, K. Mischaikow, and T. Ogawa, *Rigorous Numerics for Global Dynamics: A Study of the Swift-Hohenberg Equation*, SIAM J. Appl. Dyn. Syst. **4** (2005), no. 1, 1–31.

[14] S. Day, J.P. Lessard, and K. Mischaikow, *Validated continuation for equilibria of PDEs*, SIAM J. Numer. Anal **45** (2007), no. 4, 1398–1424.

[15] L.N. Trefethen et al, *Chebfun Version V5.2.1*, The Chebfun Development Team, 2015. `http://www.chebfun.org/`.

[16] O. Fogelklou, W. Tucker, G. Kreiss, and M. Siklosi, *A computer-assisted proof of the existence of solutions to a boundary value problem with an integral boundary condition*, Communications in Nonlinear Science and Numerical Simulation **16** (2011), 1227–1243.

[17] M. Gameiro, T. Gedeon, W. Kalies, H. Kokubu, K. Mischaikow, and H. Oka, *Topological Horseshoes of Traveling Waves for a Fast-Slow Predator-Prey System*, Journal of Dynamics and Differential Equations **19** (2007), no. 3, 623–654.

[18] M. Gameiro and J.P. Lessard., *Analytic estimates and rigorous continuation for equilibria of higher-dimensional PDEs*, J. Differential Equations **249** (2010), no. 9, 2237–2268.

[19] A. Hungria, J.P. Lessard, and J.D. Mireles-James, *Rigorous Numerics for Analytic Solutions of Differential Equations: the Radii Polynomial Approach* (2014).

[20] J.P. Lessard, J.D. Mireles-James, and J. Ransford, *Automatic differentiation for Fourier series and the radii polynomial approach* (2015).

[21] J.P. Lessard, J.D. Mireles-James, and C. Reinhardt, *Numerical Implementation of Computer Assisted Proof of Saddle-to-Saddle Connecting Orbits in IntLab*, 2012. `http://www.math.rutgers.edu/~jmireles/saddleToSaddlePage.html`.

[22] ———, *Computer assisted proof of transverse saddle-to-saddle connecting orbits for first order vector fields*, Journal of Dynamics and Differential Equations **26** (2014), no. 2, 267–313.

[23] J.P. Lessard and C. Reinhardt, *Rigorous Numerics for Nonlinear Differential Equations using Chebyshev Series*, SIAM J. Numer. Anal **52** (2013), no. 1, 1–22.

[24] R. Lohner, *Computations of Guaranteed Enclosures for the Solutions of Ordinary Initial and Boundary Value Problems*, Computational Ordinary Differential Equations, Oxford: Clarendon Press (1992), 425–435.

[25] J. Mason and D. Hanscomb, *Chebyshev Polynomials*, Chapman and Hall, 2002.

[26] R. Pachon, P. Gonnet, and J. van Deun, *Robust rational interpolation and least-squares*, Electronic Transactions of Numerical Analysis **38** (2011).

[27] ———, *Fast and stable rational interpolation in roots of unity and Chebyshev points*, SIAM J. Numer. Anal **50** (2012), no. 3, 1713–1734.

[28] L.N. Rump, *INTLAB - INTerval LABoratory*, Developments in Reliable Computing, 1999, pp. 77–104. `http://www.ti3.tuhh.de/rump/`.

[29] L.N. Trefethen, *Approximation Theory and Approximation Practice*, SIAM, 2013.

[30] J.B. van den Berg, A. Deschenes, J.P. Lessard, and J.D. Mireles-James, *Stationary Coexistence of Hexagons and Rolls via Rigorous Computations*, SIAM J. Appl. Dyn. Syst **14** (2015), no. 2, 942–979.

[31] J.B. van den Berg, C.M. Groothedde, and J.F. Williams, *Rigorous Computation of a Radially Symmetric Localized Solution in a Ginzburg-Landau P roblem*, SIAM J. Appl. Dyn. Syst **14** (2015), no. 1, 423–447.

[32] J.B. van den Berg, J.P. Lessard, and K. Mischaikow, *Global smooth solution curves using rigorous branch following*, Mathematics of Computation **79** (2010), no. 271, 1565–1584.

[33] J.B. van den Berg, J.P. Lessard, K. Mischaikow, and J.D.Mireles-James, *Rigorous numerics for symmetric connecting orbits: even homoclinics of the Gray-Scott equation*, SIAM J. on Math. Analysis **43** (2011), no. 4, 1557–1594.

[34] J.B. van den Berg and R.S.S. Sheombarsing, *MATLAB Code for Rigorous numerics for ODEs using Chebyshev-series and domain decomposition*, 2015. `http://www.few.vu.nl/~janbouwe/code/domaindecomposition`.

[35] M. Webb, *Computing Complex Singularities of Differential Equations with Chebfun*, SIAM Undergraduate Research Online (2013).

[36] D. Wilczak and P. Zgliczynski, *Heteroclinic Connections Between Periodic Orbits in Planar Restricted Circular Three-Body Problem - A Computer Assisted Proof*, Communications in Mathematical Physics **234** (2003), no. 1, 37–75.

[37] N. Yamamoto, *A Numerical Verification Method for Solutions of BVPs with Local Uniqueness by Banach's Fixed Point Theorem*, SIAM J. Numer. Anal **35** (1998), no. 5, 2004–2013.